

Electricity generation feasibility study on the Arenberg watermill

Tibo Geenen

Thesis submitted for the degree of
Master of Science in
Electrical Engineering, option Power
Systems and Automation

Supervisor:

Prof. dr. ir. Johan Driesen

Assessors:

Prof. dr. ir. Wim Dehaene

Prof. dr. ir. Ruth Vazquez Sabariego

Assistant-supervisors:

Ing. Bruno Motten

Ir. Oscar Delbeke

© Copyright KU Leuven

Without written permission of the supervisor and the author it is forbidden to reproduce or adapt in any form or by any means any part of this publication. Requests for obtaining the right to reproduce or utilize parts of this publication should be addressed to Departement Elektrotechniek, Kasteelpark Arenberg 10 postbus 2440, B-3001 Heverlee, +32-16-321130 or by email info@esat.kuleuven.be.

A written permission of the supervisor is also required to use the methods, products, schematics and programmes described in this work for industrial or commercial use, and for submitting this publication in scientific contests.

Preface

This thesis is the result of countless hours of research and the pinnacle of many projects and courses at the KU Leuven Faculty of Engineering Science, for which I am incredibly grateful towards my professors and teaching assistants. Moreover, I am honoured to have been a part of this institution.

First, I would like to thank my supervisor Johan Driesen for allowing me to work on this incredibly interesting topic and for your guidance throughout this research. I also want to express my gratitude to my assessors Ruth Vazquez Sabariego and Wim Dehaene, for reading and evaluating this thesis as the last part of my degree.

Second, my sincere gratitude goes out to Bruno Motten for always being available either for practical support or general guidance. To Kristof Engelen and Johan De Winter for your insights into practical implementations of measurements, the actual fabrication of those setups and general guidance. To Oscar Delbeke for proofreading this thesis and for your suggestions to improve the work delivered. This thesis would not have been possible without any of you.

Next, I want to thank Mathias Vaes of the VMM for allowing me to visit the Egenhoven control station and for your insights into the practical workings of such stations.

Finally, my gratitude goes out to my friends, family and girlfriend for their support throughout the past year.

In particular, I want to name my parents Seppe Geenen and Ann Lemmens who have shown nothing but love, patience and support not only during this thesis, but throughout my entire lifetime. I could not be more proud to be your son. I dedicate this work to them.

Tibo Geenen

Contents

Preface	i
Abstract	iv
List of Figures and Tables	v
List of Abbreviations and Symbols	viii
1 Introduction	1
1.1 Literature review	2
1.2 Aim and scope	10
2 Site description	13
2.1 Brief history	13
2.2 Current setup	14
2.3 VMM stations	18
2.4 KU Leuven study	22
2.5 Conclusion	23
3 Rotational speed	24
3.1 Theory	24
3.2 Practical implementation: custom tachometer	25
3.3 Data curation	26
3.4 Results	27
3.5 Inconsistent rotation	28
3.6 Conclusion	31
4 Modelling	32
4.1 Data curation	32
4.2 Data alignment	33
4.3 Regression analysis	37
4.4 Model usage	41
4.5 Conclusion	43
5 Torque	45
5.1 Theory	45
5.2 Practical implementation: hinged Prony brake	49
5.3 OCR	52
5.4 Results	56
5.5 Conclusion	58

6 Power	59
6.1 Water wheels	59
6.2 Hydraulic	61
6.3 Efficiency	62
6.4 Conclusion	62
7 Website	64
7.1 Custom tachometer v2	64
7.2 Framework	66
7.3 Operational functionality	66
7.4 Conclusion	66
8 Conclusion	67
8.1 Future work	68
A VMM stations	70
A.1 Station K08_012 - water levels	70
A.2 Maps	71
B Custom tachometer	72
B.1 Version 1	72
B.2 Version 2	73
C Modelling	74
C.1 Quality levels VMM	74
C.2 Flowchart	75
C.3 Extra plots	76
D Rubber wheel sizing	78
E Torque	79
E.1 Seven segment OCR	79
E.2 Measurements	81
F Website screenshots	82
Bibliography	84

Abstract

The Arenberg watermill located in Leuven, Belgium was restored in 2020 for aesthetic purposes after a successful crowdfunding campaign by the KU Leuven. Because the undershot water wheels rotated faster than expected, more research was requested into the possibility of electricity generation.

This thesis looks into the possible mechanical power production and efficiency of the water wheels. Measurements are taken at the axle to provide accurate estimation methods to investigate these parameters.

First, the rotational speed is constantly logged for several months to gather a vast amount of data. This data is used to investigate rotational inconsistency i.e. speed variations in a single rotation. Multiple hypotheses are tested and rotational imbalance is marked as the cause. Additionally, the data is utilised to produce a model that characterises a relationship between the rotational speed and river parameters provided by the Vlaamse Milieumaatschappij (VMM). The river parameter with the largest influence is identified to be the flow rate. Because this parameter is not directly available, the water level is used as an intermediary. This is possible as a relationship between the river parameters is observed. It implies the model is valid only under certain river conditions as this relationship changes over time. Inherent inaccuracies in the model are attributed to the unpredictability of debris caught in a trash rack placed at the water inlet.

Second, multiple torque/speed curves are characterised using an adapted version of the Prony brake method using a crane scale. Due to difficulties that hinders a typical instant dynamic torque measurement, the average dynamic torque over a full rotation is measured. Optical character recognition (OCR) software is developed for the seven segment crane scale display to facilitate constant torque logging.

Finally, the power curves are calculated together with their corresponding maximum powers. In conjunction with the hydraulic input power, efficiency values of around 10% are found. Higher efficiencies are possible to which multiple improvements are proposed. Due to temporary draught conditions, not enough power data could be measured and therefore no definite answer on the financial feasibility of the site can be produced. However, the framework built during this thesis allows certitude by additional measurements after river conditions improve.

List of Figures and Tables

List of Figures

1.1	Installed capacity for hydro, wind and solar in Europe [7]	2
1.2	Operational ranges of several hydroelectric machines [12]	3
1.3	Water wheels - types according to the water flow character[13]	4
1.4	Water wheels - general terminology [14]	5
1.5	Water wheels - Poncelet [16]	6
1.6	Water wheels - radial [17]	6
1.7	Water wheels - Zuppinger [18]	6
1.8	Water wheels - Sagebiel	7
1.9	Water wheels - number of blades n in function of radius R [5]	7
1.10	Trash rack cleaning types	8
1.11	The Archimedes screw [12]	9
2.1	Arenberg site - 1900 [31]	14
2.2	Arenberg site - 2017 [33]	14
2.3	Arenberg site - 2020 - including name assignments [34]	14
2.4	Arenberg site - location relative to the river Dyle	15
2.5	Arenberg water wheel - technical drawing (provided by the KUL)	16
2.6	Arenberg water wheel - axle ends inside the mill building	17
2.7	Example of an inflow weir and its characteristics	18
2.8	Arenberg site - location of the closest VMM stations	19
2.9	Station K08_012 - local monitoring system of river parameters	19
2.10	Station K08_012 - pneumatic valves	20
2.11	Station K08_012 - gate types to control downstream water level	20
2.12	Station K08_012 - limnigraph used to measure water levels	21
2.13	Station K08_012 - upstream flood area [39]	22
2.14	Station K08_012 - downstream sediment trap [40]	22
2.15	Arenberg site - zones influenced by former target water level [39]	23
3.1	Custom tachometer - v1 - installation	25
3.2	Modelling flowchart - data curation rotational speed	26
3.3	Rotational speed - raw data	27
3.4	Rotational speed - timestamped	28

LIST OF FIGURES AND TABLES

3.5	Rotating object imbalance visualisation	29
3.6	Arenberg water wheel - equally spaced trigger points	29
3.7	Rotational speed - measurements inconsistent rotation	30
4.1	Modelling flowchart - river parameter processing	32
4.2	Modelling flowchart - quarter-hour ν intervals	33
4.3	Modelling flowchart - data alignment	34
4.4	Rotational speed - function of head - Volmolen-Egenhoven	34
4.5	Rotational speed - function of flow rate - SJW	35
4.6	Relationship between flow rate and water level $Q(h)$ - SJW	35
4.7	Rotational speed - function of water level - Egenhoven	36
4.8	Modelling flowchart - regression analysis	37
4.9	Arenberg site - trash rack with built-up debris	37
4.10	Rotational speed - function of water level - data bins	38
4.11	Rotational speed - mill 1 - function of water level - final model	40
4.12	Rotational speed - mill 2 - function of water level - final model	41
4.13	Modelling flowchart - retrospective estimation	41
4.14	Band around $Q(h)$ to validate the final model - SJW	43
5.1	Theoretical method torque - torque transducer - strain gauge [51]	46
5.2	Theoretical method torque - Prony brake - basic implementations	47
5.3	Theoretical method torque - Prony brake - belt and dual scales	47
5.4	Theoretical method torque - Prony brake - hinged	48
5.5	Theoretical method torque - motor test bench [58]	49
5.6	Practical method torque - hinged Prony brake	50
5.7	Rotational speed - handheld tachometer	50
5.8	Practical method torque - hinged Prony brake - spring	51
5.9	Preprocessing & OCR flowchart - crane scale seven segment display	53
5.10	Crane scale frame - original isolated blue channel	54
5.11	Crane scale frame - cutoff isolated blue channel	54
5.12	Crane scale frame - original vs preprocessed	54
5.13	Seven segment display theory	55
5.14	Seven segment OCR - frame detection	56
5.15	Arenberg water wheel - force evolution for one full rotation	57
5.16	Arenberg water wheel - torque/speed curves	58
6.1	Arenberg water wheel - power curves	60
7.1	Custom tachometer - v2 - 3D model	65
7.2	Custom tachometer - v2 - installation	65
A.1	Station K08_012 - downstream water levels and threshold of 23.5 mTAW	70
A.2	Station K08_012 - upstream water levels and filling stages of flood area	70
A.3	Arenberg site - location of the closest VMM stations - including SJW	71
B.1	Custom tachometer - v1 - circuit diagram	72

LIST OF FIGURES AND TABLES

B.2	Custom tachometer - v2 - circuit diagram	73
B.3	Custom tachometer - v2 - internal wiring	73
C.1	Modelling flowchart - all operations on the rotational speed and river data	75
C.2	Rotational speed - function of water level - Volmolen	76
C.3	Rotational speed - function of water level - final model - residuals	76
C.4	Q(h) data points divided in winter and summer - SJW	77
C.5	Station K08_012 - forecasted water levels - Egenhoven	77
D.1	Rubber wheel to increase the rotational speed - calculation	78
E.1	Crane scale frame - intermediate steps	79
E.2	Seven segment OCR - flaw - full digit removed	80
E.3	Seven segment OCR - flaw - half of digit removed	80
E.4	Arenberg water wheel - torque data points	81
E.5	Residuals for quadratic fit for $T_{\nu_{0.85}}$	81
E.6	Residuals for quadratic fit for $T_{\nu_{1.05}}$	81
F.1	Arenberg watermill website - homepage	82
F.2	Arenberg watermill website - real-time - mill 1	83
F.3	Arenberg watermill website - real-time - graph	83

List of Tables

1.1	Hydropower categories by power range according to UNIDO [5]	3
1.2	Water wheels - theoretical and measured efficiencies by undershot subtype [15, 16, 19, 23]	7
1.3	Published papers over the last decades on water wheels. T = theoretical work, E = experimental work and N = numerical solutions [5]	12
6.1	No-load rotational speeds ν_{nl} with corresponding rotational speed set points, maximum power points, hydraulic powers and efficiencies	62
C.1	Quality codes - VMM data	74

List of Abbreviations and Symbols

Abbreviations

CV	Coefficient of variation
EU	European Union
IoT	Internet of things
K08_012	Code for Egenhoven uitlaatkunstwerk
KUL	Katholieke Universiteit Leuven (Catholic University of Leuven)
LUT	Lookup table
MPPT	Maximum power point tracking
NaN	Not a number
OCR	Optical character recognition
RGB	Red, Green and Blue
RTC	Real-time clock
SJW	Sint-Joris-Weert
UNIDO	United Nations Industrial Development Organisation
VMM	Vlaamse Milieumaatschappij (Flanders Environment Agency)

Symbols

A	Water flow surface of turbine
CV_h	Coefficient of variation in water level in a single day
g	Standard gravity
H	Head
h	Water level
L	Lever arm length Prony brake
m	Mass of compensating weight in a Prony brake
n	Number of blades of a water wheel
N	Number of water level measurements in a single day
P_{in}	Power available in the water
P_{max}	Maximum mechanical power provided by a water wheel determined by MPPT
P_{mech}	Mechanical power provided by a water wheel
ρ	Water density
Q	Flow rate
R	Radius of a water wheel
T	Torque
u	Tangential velocity at the tip of a blade
ν	Rotational speed [r/min]
ν_1	Rotational speed of mill 1
ν_2	Rotational speed of mill 2
ν_l	Load rotational speed
ν_{max}	Rotational speed at which the power is at its maximum in MPPT
ν_{nl}	No-load rotational speed
v	Water flow velocity
w	Resulting flow velocity
ω	Angular frequency

Chapter 1

Introduction

The introduction of resource-independent renewables is arguably the most pressing technical challenge we face as the human race at the moment. The necessity of green energy is not only showing in the more increasingly prevalent climate change, but is also seen in more recent geopolitical situations. This is especially true for countries in the European Union (EU). The Russian invasion of Ukraine in late February 2022 has led to an even higher peak in the already rising energy prices and will most likely influence the energy markets for some time. As long as the EU is highly dependent on Russian resources and geopolitical conflicts remain present, those resources can be used as a significant bargaining chip to counter imposed sanctions. In 2020, the EU imports from Russia reached up to 43 % for natural gas, 29 % for crude oil and 54 % for coal of their total import [1]. In response to these threats, the EU has launched multiple initiatives such as the well-known European Green Deal and REPowerEU. Both of them contain the increase in green energy production as a primary objective [2, 3].

The most discussed and used forms of renewable power in the EU are wind, hydro and solar with 36 %, 33 % and 14 % of the renewable energy production in 2020 respectively [4]. However, European investments in hydropower have become stagnant over the past decade while solar and wind have increased significantly as can be seen in Figure 1.1. This is not to say hydro is not an important source of electrical energy any more, as it remains the largest in installed capacity and is responsible for a third of the renewable energy production in Europe. It does however seem likely that wind and solar will overtake this position should the current investment trend continue. The main reason for this is the scarcity of high power hydro. Firstly, because most of the suitable sites have already been exploited and secondly because of their large environmental impact [5]. Another reason is the distorted market, because wind and solar are subsidised heavily [6]. Smaller hydropower plants on the other hand are not common, but could be interesting because of their low environmental impact and thus potentially revitalise European investments in hydropower.

Additionally, infrastructure costs can be significantly reduced if existing sites are exploited [8]. Prior to the industrial revolution, traditional hydropower techniques

1. INTRODUCTION

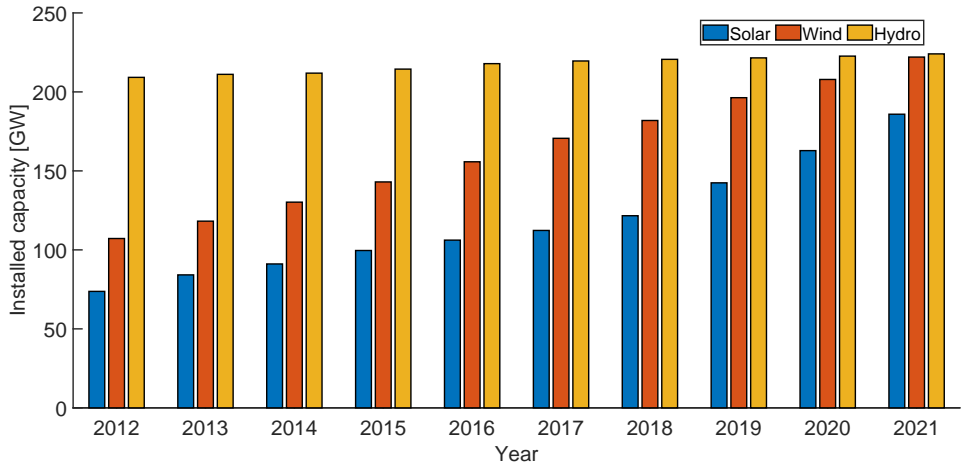


FIGURE 1.1: Installed capacity for hydro, wind and solar in Europe [7]

utilizing water wheels were prevalent and played a major role in driving the economic, industrial, and social development of rural agricultural areas. Up to 350 000 water wheels were installed in Europe alone [9, 10]. This indicates that there is a significant and untapped hydropower potential at sites with head values (i.e. the height difference between up- and downstream relative to the site) below 2.5 m in many countries. In this case, standard turbine types are deemed cost-ineffective due to the need for large turbine diameters and significant civil engineering efforts, which would ultimately still result in a relatively low power output [11]. Water wheels on the other hand are less complex and thus cheaper while still reaching high efficiencies under the right conditions. They might provide a solution to this economic infeasibility and prove their use in renewable power production. One of the remaining water wheels is the iconic “Watermolen van Arenberg” (translation: Arenberg watermill), built in 1286 and located on KU Leuven grounds in Heverlee, Belgium. This thesis looks into the economic feasibility of green electricity production by this specific watermill. Although the research is being done for a specific site, the techniques used can be performed for other feasibility studies with similar sites around the globe.

It is important to mention that this study will not try to optimise the environment of the site and will only look at the electricity generation capabilities as is. This means nor changes to the water wheel nor changes to the river can be made and the entire site should thus be studied as is. The exact reasons for this will be explained in the next chapter. However, it is still interesting to look at other technologies that may have been better suited for power production at the site.

1.1 Literature review

In order to better describe the studied site at the Arenberg water wheel, this section looks into available literature of water wheels and other low-head hydroelectric technologies. Although the site has to be studied as is, an understanding of other

1.1. Literature review

technologies is still useful to determine what the (dis)advantages of the setup are and what could have been done differently. The formulas to calculate the power of rotating machines and hydro systems are also briefly explained.

Each hydroelectric machine has its own operational range as depicted on Figure 1.2. The hydropower categories used on the figure are according to the United Nations Industrial Development Organisation (UNIDO) and are listed in Table 1.1. As described in Chapter 2, this thesis deals with a very low-head and flow rate site and will therefore focus on hydroelectric technologies suited for those conditions. More specifically, in the best case scenario the head H equals about 0.3 m and the flow rate Q about $0.3\text{ m}^3/\text{s}$ (measured directly at site). From Figure 1.2, suitable technologies therefore are undershot water wheels and Archimedes screws. These are further investigated in Section 1.1.1 and 1.1.2 respectively. These conditions yield a maximum power generation of $<1\text{ kW}$ according to the same figure, classifying the site as pico hydro according to UNIDO standards.

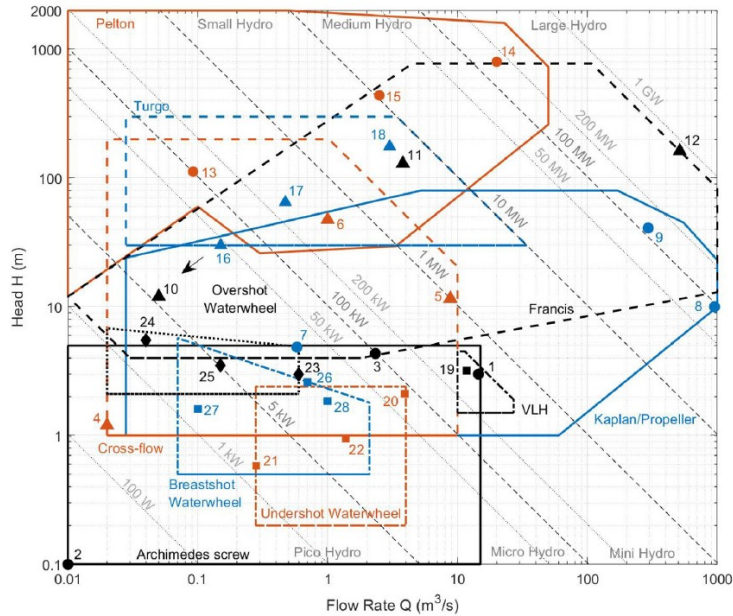


FIGURE 1.2: Operational ranges of several hydroelectric machines [12]

TABLE 1.1: Hydropower categories by power range according to UNIDO [5]

Hydropower category	Power range
Pico	$<5\text{ kW}$
Micro	$5\text{ kW} - 100\text{ kW}$
Mini	$100\text{ kW} - 1\text{ MW}$
Small	$1\text{ MW} - 10\text{ MW}$
Medium	$10\text{ MW} - 100\text{ MW}$
Large	$>1\text{ GW}$

1. INTRODUCTION

1.1.1 Water wheels

Water wheels and their power generation capabilities are the main subject of this thesis and are therefore thoroughly discussed in this section. First, the terminology is defined. Then the efficiencies of different types of undershot water wheels are discussed. This is followed by some short insight into the ideal number of blades present on a water wheel. Finally, trash racks and their influence on the environment and power generation capabilities is analysed.

Terminology

There are four main different types of water wheels according to the character of the water flow: stream, undershot, breastshot and overshot as depicted on Figure 1.3. The stream and undershot types are predominantly driven by kinetic energy retrieved from the water. The overshot is driven by gravitational potential energy, while the breastshot type is a combination of both as the water enters around axle height. Because the stream type has the same working principles as the undershot type, they are often (also in this thesis) grouped under the latter. Note that these representations are simplified and a lot of variations exist.

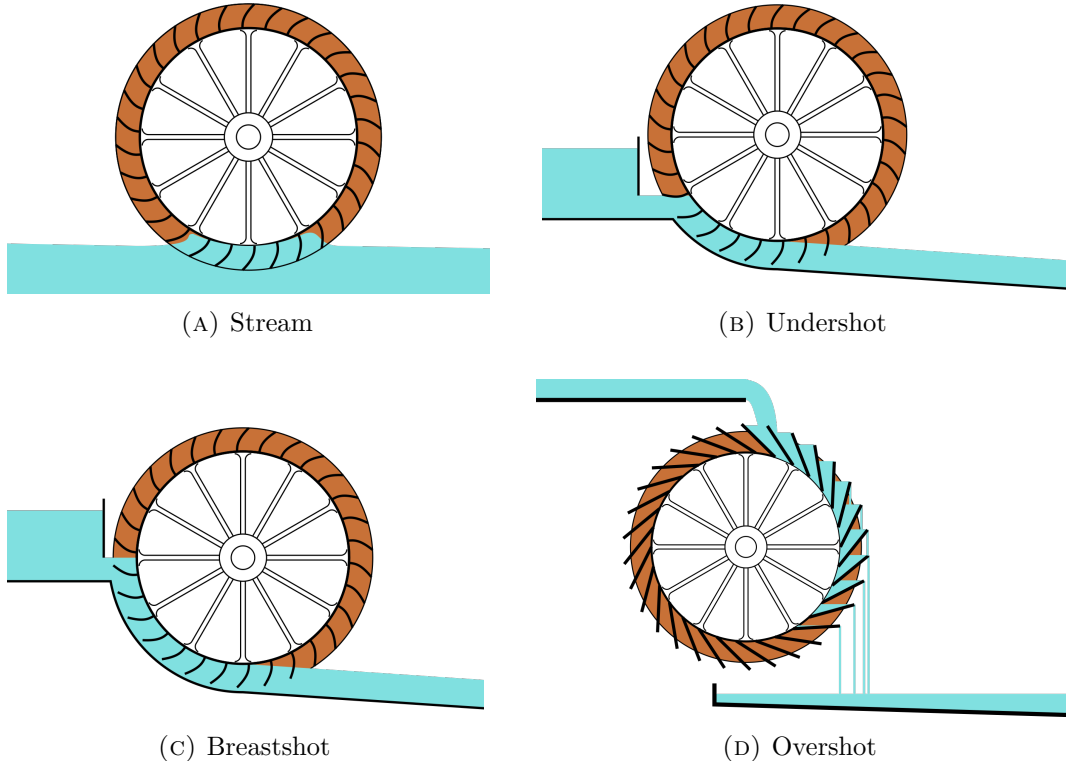


FIGURE 1.3: Water wheels - types according to the water flow character[13]

As mentioned before, the undershot type is the only suitable technology for the site and thus the only discussed type in the rest of this subsection. Before moving on,

it is important to define all the necessary terminology needed to fully understand the topic. Figure 1.4 summarises most terms used throughout this thesis concerning water wheels. As the terminology is easy to understand from the figure, no extra explanation is needed. A missing device in the figure is a trash rack, which is a screen placed upstream from the water wheel preventing fish and debris from entering the system. The trash rack will be explained more clearly later in this section. Although the figure is a representation of a breastshot type water wheel, the same terminology is used for the other types.

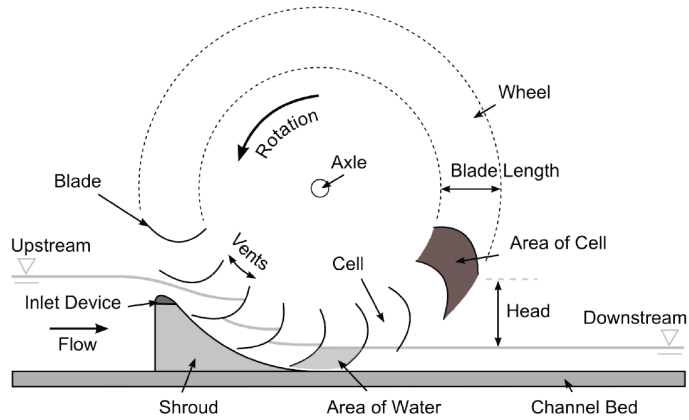


FIGURE 1.4: Water wheels - general terminology [14]

Efficiency

The most important characteristic of a water wheel is its efficiency, meaning the ratio of the mechanical power P_{mech} provided by the water wheel and the available power from the water P_{in} . These powers are defined in Section 1.1.3. Throughout history, a lot of improvements have been made to optimise the efficiency and therefore, it is interesting to look at the evolution for undershot water wheels for every subtype. This is especially true since the Arenberg water wheels are modelled after the original one built over 700 years ago.

The main working principle is the same for every subtype (i.e. driven by kinetic energy in the water), but the blade inclination and shape vary. The most straightforward and basic subtype is radial. It shows no special modifications to the blades, as shown on Figure 1.6. The blades are straight and radially placed.

The first groundbreaking modification can be seen on Figure 1.5 and was invented by J.V. Poncelet [15]. It has curved blades which is beneficial for two reasons: more of the water's momentum is transferred to the water wheel and a gravitational component is added as the water is held by the newly formed 'water buckets'. The former is true, because the water can flow from the tip to the root of the blade [5].

1. INTRODUCTION

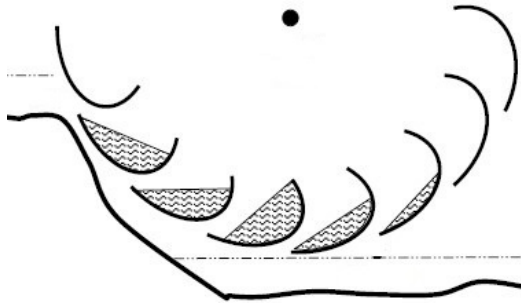


FIGURE 1.5: Water wheels - Poncelet [16]

Finally, the two most common subtypes were created: the Zuppinger and Sagebien water wheels. Zuppinger minimises the downstream power losses, because the water is not lifted upwards before it returns to the river but easily glides off the blades downstream.



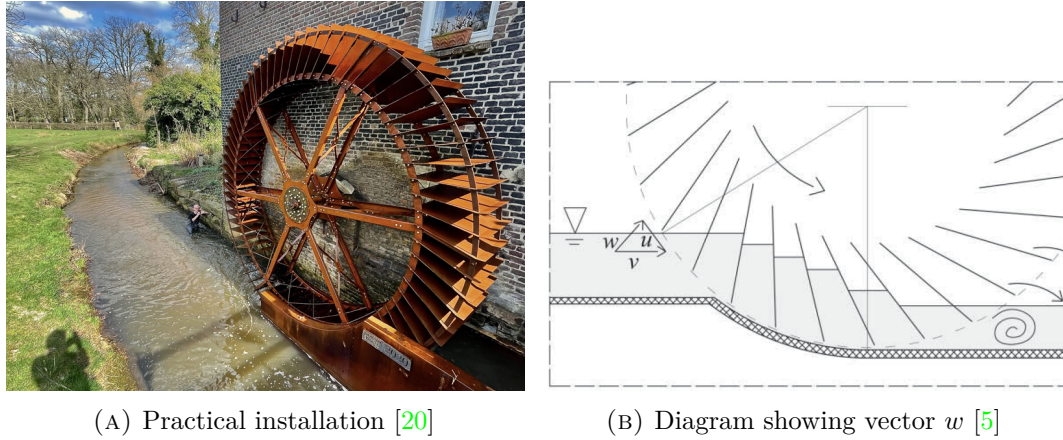
FIGURE 1.6: Water wheels - radial [17]



FIGURE 1.7: Water wheels - Zuppinger [18]

Sagebien minimises the upstream power losses by minimal disturbance of the water flow. Its blades are angled to align with the effective flow velocity vector w , which is the result of the difference between the water flow velocity vector v and the tangential velocity vector to tip of the blade u as shown in Figure 1.8b. Both subtypes lead to similar results in practice, but the Sagebien wheel is less popular because of the large number of blades leading to high production and maintenance costs [19].

These inventions incrementally lead to tremendous improvements in terms of efficiency, as shown in Table 1.2. The blade shape and inclination is clearly of great importance when it comes to efficiency of undershot water wheels. Note that the efficiency is never fixed, but also depends on river parameters such as flow rate and head according to similar research [11, 21, 22]. The measured efficiencies in the table therefore show best and worse case scenarios based on these river parameters.



(A) Practical installation [20]

 (B) Diagram showing vector w [5]

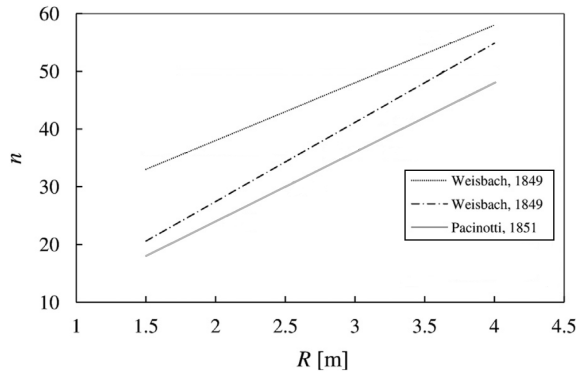
FIGURE 1.8: Water wheels - Sagebien

TABLE 1.2: Water wheels - theoretical and measured efficiencies by undershot subtype [15, 16, 19, 23]

Subtype	Efficiency η (%)		
	Theoretical	Measured	
		Worst case	Best case
Radial	30	13	22
Poncelet	50	55	63
Zuppinger	70	50	84
Sagebien	90	61	84

Number of blades

Another variable is the number of blades. Multiple proposals are made for the radial subtype in literature, but there seems to be one consensus: the number of blades n should be directly proportional to the radius R of the water wheel, as shown on Figure 1.9.

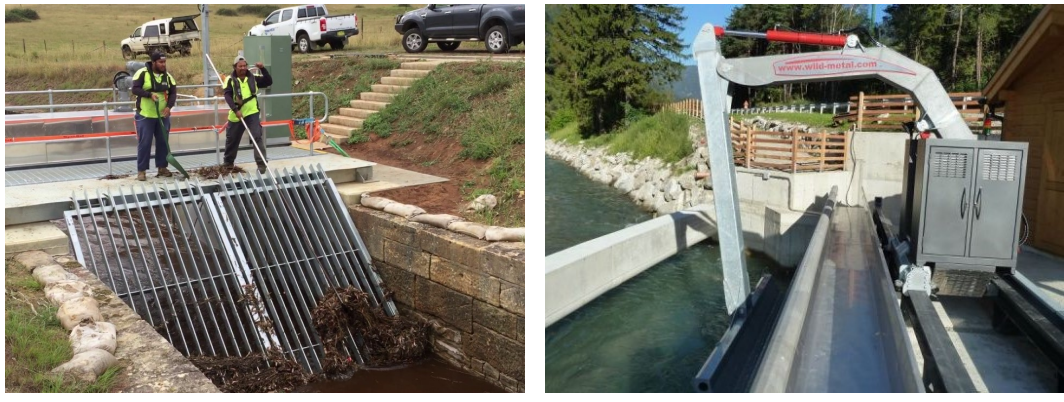

 FIGURE 1.9: Water wheels - number of blades n in function of radius R [5]

1. INTRODUCTION

The typical Zuppinger wheel has between 32-48 curved blades and a diameter between $6 - 7.5\text{ m}$, meaning there is a spacing between the blades (or length of vents) of $0.5 - 0.6\text{ m}$. The Sagebien ranges between 70-80 straight blades and $7.5 - 10\text{ m}$, leading to a spacing of $0.3 - 0.4\text{ m}$ [5].

Trash rack

A trash rack consists of vertical bars separated by gaps where the water can pass through. It is placed directly upstream from the water wheel for two reasons. First, to protect the wheel from damage by debris in the river (e.g. sediment, branches, leafs...). Second, to prevent passage from fish through the machinery that can be harmed by the rotating blades. The system should be monitored and designed carefully, because it can have severe consequences for the environment and/or the power production if too much debris builds up. This is because the head difference created across the screen can raise the upstream water level or decrease the flow rate in the system [14]. It can even cause the entire system to clog up and not allow any water to pass through at all. The system should thus be cleaned regularly, either manually as shown on Figure 1.10a or automatically with a device as shown on 1.10b. The latter is expensive, so a cost/benefit analysis is in order.



(A) Manual [24]

(B) Automatic [25]

FIGURE 1.10: Trash rack cleaning types

1.1.2 Archimedes Screws

The second possible technology for the studied site was determined to be the Archimedes screw shown on Figure 1.11. It offers two main advantages over water wheels: the efficiency reaches up to 89% [26] and it is more eco-friendly in terms of fish and sediment passage [27]. The latter advantage can contribute greatly to getting permits approved to build or renew sites, especially because the difference is fairly large in terms of fish passage. In one study, 92% of the fish passed unharmed, while this was only 72% for water wheels [28]. A direct consequence is that the trash rack in front of the Archimedes screw can be more coarse. This means that there

is less flow rate loss and debris is built up less quickly. The latter enhances the former even more in addition to less need of maintenance. These effects cannot be underestimated as shown later in Section 4.3.1.

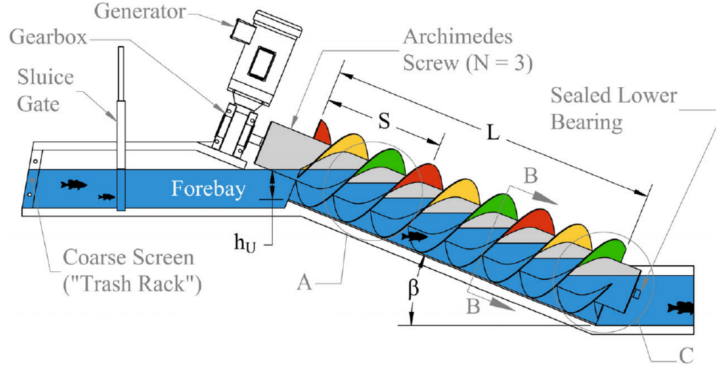


FIGURE 1.11: The Archimedes screw [12]

1.1.3 Power calculation

Mechanical power

The mechanical power P_{mech} delivered by a rotating object, regardless of the technology used, is calculated by the following formula [29]:

$$P_{mech} = T \cdot \omega \quad (1.1)$$

T represents the dynamic torque and ω represents the angular frequency.

The rotational speed ν (in r/min) is mostly used in this thesis, which holds the following relationship with ω :

$$\omega = \nu \cdot \frac{2\pi}{60} \quad (1.2)$$

Hydraulic power

The power P_{in} delivered by the water is as follows [30]:

$$P_{in} = \rho \cdot g \cdot Q \cdot H \quad (1.3)$$

The constants ρ and g represent the water density and standard gravity respectively. H denotes the head across the system and Q the flow rate in the system. It is important to note that Q has to be further dissected:

$$Q = v \cdot A \quad (1.4)$$

Where v is the water flow velocity and A the surface trough which the river flows. Both terms can vary.

1. INTRODUCTION

The formulas listed above make use of SI units only, as do all other units throughout this research unless mentioned otherwise. Four of the used variables are of great importance and will be reoccurring topics throughout this thesis: T , ν , Q and H .

Efficiency

If both P_{mech} and P_{in} are known, the efficiency η of the used technology can easily be calculated by:

$$\eta = \frac{P_{mech}}{P_{in}} \quad (1.5)$$

1.2 Aim and scope

1.2.1 Aim

As stated before, the aim of this research is to assess the (economic) feasibility of electricity generation by the Arenberg watermill without bringing any changes to the site. The assessment is performed by performing multiple measurements at the site and providing different models out of those results using MATLAB as the main programming tool.

To discuss (economic) feasibility, it is necessary to determine the power production capabilities of the water wheels. To be able to do this, two important measurements are needed: the rotational speed and the torque. Multiplying those terms yields the instantaneous mechanical power delivered by the wheels according to Equation 1.1. Performing tests at random points in time would not allow an immediate conclusion though. River water is subject to a lot of external factors such as precipitation, extreme heat causing draught, human control to prevent flooding... Therefore, measurements should be performed over a longer time period so models can be made to characterise the water wheel data in terms of the river parameters. The different measurements and their respective models are listed in the subsections below.

Rotational speed

The most important data to be measured is the rotational speed of the water wheels ν . It is the most straightforward way of measuring the influence of river parameters on the power generation. This thesis will attempt to use publicly available water level and flow rate data to create a model that characterises rotational speed in function of this river data. The rotational no-load speed will therefore be measured during the duration of the research.

Torque

Torque is a lot harder to measure over long periods of time. Instead, it is far easier to characterise the torque/speed curve of the water wheel. That way the torque

is always known based on the no-load speed and also indirectly linked to the river parameters through the model described above. Most importantly the power curve is inherently present in the torque/speed curve data as it is the product of both terms.

Power

Based on the power curves, a set point can be found to maximise the power generated for all river properties. This principle is very much the same as the maximum power point tracking performed for solar panels, meaning well-established algorithms could be used to force the generator into the optimal power producing set point.

Energy

Knowing the power generation capabilities based on river data, opens up the opportunity to make a best/worse case scenario of the possible yearly energy production. This can be done by finding the year with the lowest and highest water levels and/or flow rates, estimating the rotational speed from this data, finding the optimal power point and lastly multiplying the power by the time interval of the dataset. Note that at this point in time, the only known energy is purely mechanical. Taking into account the losses of the possible gearbox, power electronics... by multiplying their efficiencies with the mechanical energy yields the final electrical energy produced.

Financial analysis

A financial analysis is possible knowing the investment costs needed to generate power, the amount of electrical energy produced over some time and the cost of the same amount of energy. The payback period and the ROI over its lifetime can be estimated too.

Unfortunately, not enough torque/speed curves at different no-load speeds were characterised due to severe drought during this research. This makes it impossible to perform any meaningful financial analysis as the power and thus the energy at most no-load speeds is still unknown. Some aims are therefore only partially researched and the remainder is marked as future work.

1.2.2 Scope

Although water wheels are not a popular method of electricity production, there has been a renewed academic interest over the last decade or so due to the more pressing need for an energy transition. As mentioned before, there are still a lot of sites left with untapped very low-head hydropower capabilities that could be put to good use in this transition. An oversight of the most prevalent papers published in the last decades is shown in Table 1.3.

1. INTRODUCTION

TABLE 1.3: Published papers over the last decades on water wheels. T = theoretical work, E = experimental work and N = numerical solutions [5]

Authors	Year	Institution	Country	Overshot	Breastshot	Undershot
Williams and Bromley	2000	Nottingham Trent University	UK	T E		
Müller and Kauppert	2002-2004	Southampton University	UK	E	E	
Müller and Wolter	2004	Southampton University	UK		T E	E
Dubas	2005	Haute Ecole Valaisanne	France	T E		
Wahyudi et al.	2013	Polytechnic of Malang	Indonesia	E		
Von Harten et al.	2013	University of Stuttgart	Germany			E
Pellicciardi	2015	University of Siena	Italy	T E		
Quaranta and Revelli	2015	Politecnico di Torino	Italy	T E		
Quaranta and Revelli	2015–2016	Politecnico di Torino	Italy		T E	T E
Vidali et al.	2016	Politecnico di Torino	Italy	T E		
Quaranta and Revelli	2016	Politecnico di Torino	Italy			N
Quaranta	2017	Politecnico di Torino	Italy			N
Quaranta and Müller	2017	Politecnico di Torino- Southampton University	Italy-UK			E
Paudel et al.	2017	Darmstadt University of Applied Sciences	Germany			E

Ongoing research projects on (undershot) water wheels exist, but they are few and often only performed in a controlled test environment. That is exactly where this thesis differentiates itself from the rest of the research being done. None of the data measured is in a controlled environment and thus subject to all sorts of external factors. Additionally, none of the papers listed provide any clue as to how a type of water wheel links to river water levels or flow rates and none of them provide any torque/speed characteristics. Therefore, this thesis will attempt to provide new insights into the practical workings of undershot water wheels.

Chapter 2

Site description

This chapter gives a detailed description on the site, as well as insight into relevant operations in its immediate surroundings. First, it briefly introduces the historical significance of Arenberg site. This is followed by the description of the site and the specific water wheel to provide a clear image of what is being studied. Then, measuring stations in the surroundings of the site are explained in detail. Finally, previous studies performed by the KU Leuven are summarised to underline the importance of the environment in this study and the reasons why the site cannot be changed.

2.1 Brief history

The first record of the Arenberg water wheels (or watermills) dates back to 1286, but when exactly it was built is not known. In those days, there were two wheels in use placed at opposite sides of the river bed: one for grinding grain and one for sawing wood. The latter was retired in the beginning of the 17th century and later rebuilt on the other side of the river bed. Figure 2.1 shows the site before the second wheel was rebuilt with the castle of Arenberg in the background. After being in the hands of dukes van Croÿ and van Arenberg, the Catholic University of Leuven (KUL) took over in 1923 and quite literally kept the wheels turning until 1958. The mill building was cleared and renovated to serve as offices and classrooms, but the water wheel stayed in place for purely aesthetic purposes. They were even classified as a protected monument in 1999 [31], but as the years went by the wheels were in desperate need of restoration as seen in Figure 2.2. The KU Leuven therefore launched a successful crowdfunding campaign in 2017 bringing in over €200.000 in addition to the same amount already pledged by the university itself [32].

The original plan was to generate green electricity, but a preliminary study proved this to be improbable as seen in Section 2.4. Therefore, a purely aesthetical restoration was decided for with the hopes of letting the wheels turn freely without any power generation. The water wheels were restored in their full glory and original design in 2020 as shown on Figure 2.3. To the delight of many, the wheels did turn and even

2. SITE DESCRIPTION

faster than expected renewing the question if the water wheels can ever be used for power generating purposes.



FIGURE 2.1: Arenberg site - 1900 [31]



FIGURE 2.2: Arenberg site - 2017 [33]



FIGURE 2.3: Arenberg site - 2020 - including name assignments [34]

2.2 Current setup

The Arenberg site is located in Heverlee, a municipality of Leuven, Belgium next to the river Dyle. Its exact location and the entire river course is shown on Figure 2.4. The wheels are located on the west side of the river and are placed next to each other as shown on Figure 2.3. To make a distinction between both mills, a number is assigned to each one: the wheel closest to the mill building is number 1, the other is number 2.

About 1 km up- and downstream from the mill building, there are measuring/control stations operated by the Vlaamse Milieumaatschappij (VMM) (translation: Flanders Environment Agency). Several parameters are measured such as water level, flow

2.2. Current setup

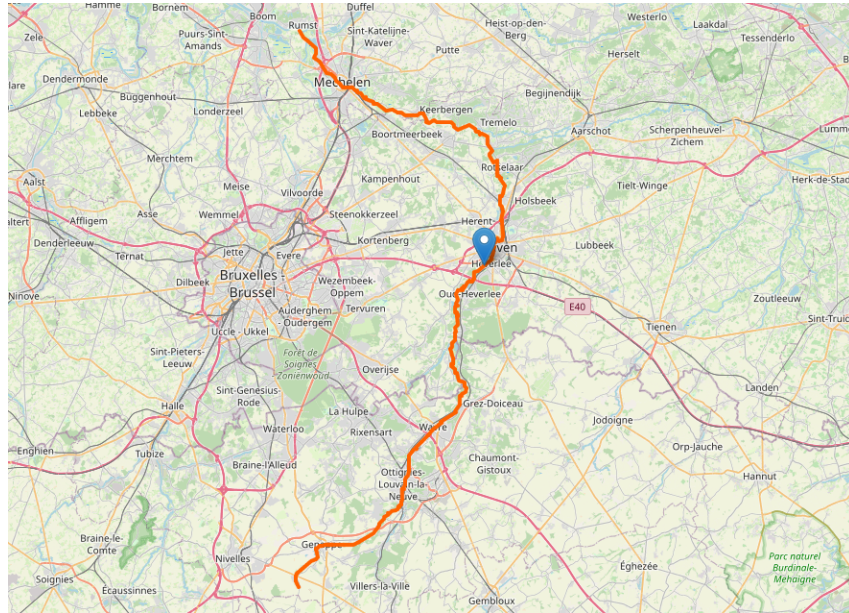


FIGURE 2.4: Arenberg site - location relative to the river Dyle

rate, precipitation, etc. to, among other goals, make sure floods and water shortages are kept under control. Based on those measurements, some stations can be used to control the water level upstream, so that the cities downstream are not flooded. The measurement data is public and of great importance to realise some models developed in this thesis discussed in Chapter 4. In context of the research being done, a site visit was arranged with the VMM and described in Section 2.3.

2.2.1 The water wheels

The water wheels at the Arenberg site need to be described both on the out- and inside to understand what is being researched. Although the site cannot be changed, this allows for some interesting insights into possible improvements.

Outside description

As mentioned before, the restoration works focused on aesthetics and not functionality. This means the water wheel was modelled after the original one, without taking into account the ideal inclination and or shape of the blades as discussed in Section 1.1.1. A technical drawing is shown on Figure 2.5. The radius R from the centre of the axle to the tip of a blade is 2.53 m . There are 40 straight blades present that are inclined under an angle of 13° . Depending on the depth of the water at the inlet, the design has a lot of similarities with the Sagebien subtype. Additionally, the spacing between the blades is equal to 0.397 m which fits perfectly into the range of an ideal Sagebien wheel. If the water wheel is placed correctly and the water is entered under the right angle, the efficiency could theoretically reach up to 90%.

2. SITE DESCRIPTION

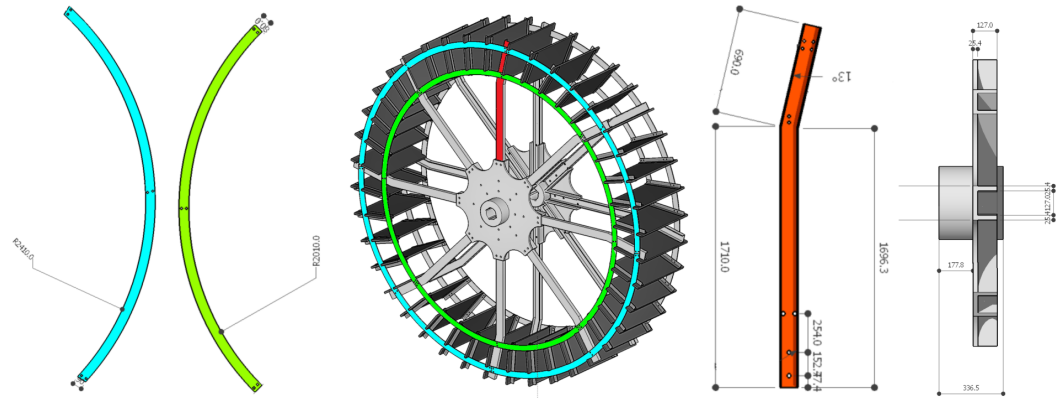


FIGURE 2.5: Arenberg water wheel - technical drawing (provided by the KUL)

The water wheels are separated from each other and from the main river by brick walls, forming a channel just wide enough for the blades to pass through. Just upstream from the water wheels, there is a small natural water drop creating a very-low head across the water wheels. A few wooden planks were placed at the drop to increase the head slightly, but no additional control is allowed as will be discussed in the next section. Mill 1 is placed slightly closer to the drop and therefore experiences a slightly larger head.

A trash rack is placed just upstream from the mills which has a significant impact on the rotational speed (and therefore power) as will be discussed in Chapter 4. Part of the river water flows through the trash rack, but most of it flows away freely with the main river never reaching the water wheels.

Inside description

Both axles are running into the mill building and end in a well, formed by a cutout of the cement floor. Attached to the axle ends are smaller wooden wheels that can be used to slow down or even put the entire water wheel to a halt. A belt coated with a rubber-like material can be pulled tighter around the wooden wheel, causing the movement to stop by friction. This principle will be used later on in Chapter 5 to measure the torque. The axle ends can be seen on Figure 2.6.

The wooden wheels are not perfectly round with a minimum radius of 0.545 m and a maximum radius of 0.562 m. This difference will become relevant in Section 5.2.2.



FIGURE 2.6: Arenberg water wheel - axle ends inside the mill building

Possible improvements

In practice, the water wheel does not provide the advantages of any subtype. Figure 2.3 was taken from the upstream point of view, looking toward the downstream river. This means that instead of the blades being inclined toward the water surface like the Sagebien design, they are inclined away from it. Figure 2.2 shows that the water wheels were originally installed that way before the restoration. This is probably the reason they were restored and placed like they are now, with adverse consequences for the wheel efficiency. When the wheels were still in use, the head was significantly larger than it is now and they were most likely classified as a breastshot wheel.

With the current placement, the biggest disadvantages of both the Zuppinger and the Sagebien subtypes are combined: higher disturbance of the flow upstream by misalignment with the flow velocity vector w and more resistance downstream by lifting the water upwards. There is a straightforward solution to this problem: rotating the water wheels around the z-axis by 180° .

However, even if the wheel is flipped around there would still have to be other adaptations. The angle at which the blades enter the water does not only depend on the blade position, but also on the height of the water. The current setup does not control the local water level directly upstream from the system. This would be possible by the placement of an inflow weir as shown on Figure 2.7a. This weir would not influence the upstream water level because there is an instant drop at the site location already present. Several types of weirs exist with their own rating curve showing the water level at the inlet device in function of the flow rate of the river. An example of such a rating curve is shown on Figure 2.7b. The ideal weir in this

2. SITE DESCRIPTION

setup would have a flat curve so that there is little variability in water level over a large flow rate range. That way, the ideal water level can be determined and kept fairly constant so that the blades enter the water under the right angle. In practice, it is difficult to design such an ideal weir, but adjustable inflow weirs with different rating curve settings can be implemented [21].

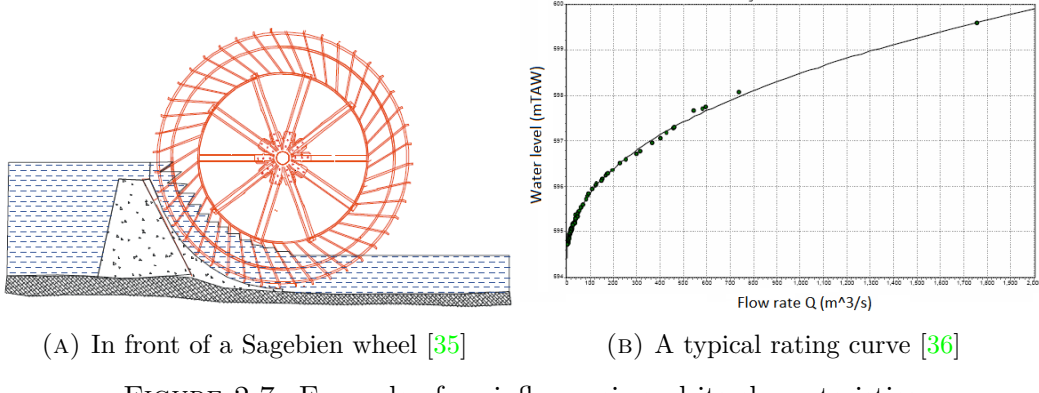


FIGURE 2.7: Example of an inflow weir and its characteristics

Without these improvements, the water wheel can be best described by a radial subtype. This is because in general the local water level is low and the blades are only slightly angled (in the wrong direction) so that the water is cut similarly as a radial subtype would. This means the efficiency is about 4 times lower than it could be, as shown in Table 1.2 in Section 1.1.1.

Another improvement from both a maintenance/lifetime and operational point of view would be to balance out the water wheel. Section 3.5 proves rotational imbalance is present and discusses the consequences should this not be fixed. The imbalance can be solved by either adding mass at certain locations around the wheel or removing mass at the opposite site of those locations. Finding these locations is considered out of scope, as the site is studied as is.

2.3 VMM stations

As mentioned before, the VMM has measuring/control stations at several points on the Dyle (and all around Flanders). Figure 2.8 shows the locations of the closest measuring stations up- and downstream of the mill. To get a better understanding of how the data is being measured and what the consequences would be if the water level would not be controlled, a site visit was planned at one specific station: “Egenhoven uitlaatkunstwerk” or station K08_012. The reason why this station was selected will become clear in Section 4.2.3.

2.3.1 Water level control

Also visible on Figure 2.8 is a part of the city of Leuven through which the Dyle flows. In case of extreme weather conditions, the water level of the Dyle might rise

2.3. VMM stations

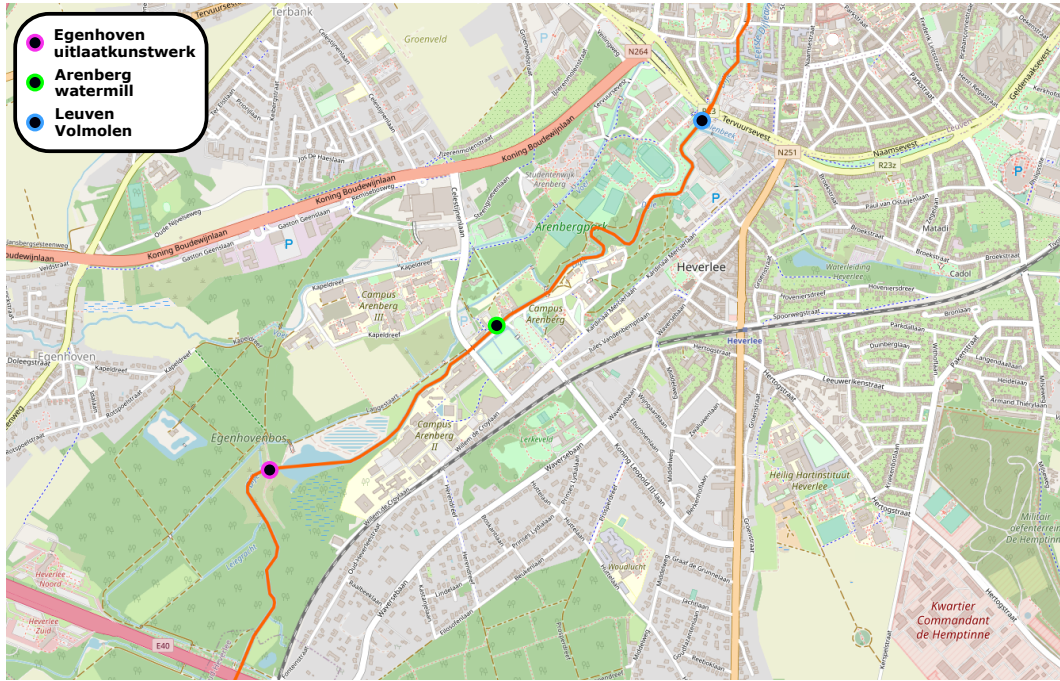


FIGURE 2.8: Arenberg site - location of the closest VMM stations

significantly causing flooding and possible damages to the city. To prevent this from happening, the water level is carefully monitored along different points of the river. If the water level rises up to a certain point, the VMM takes precautions upstream by controlling pneumatic valves in a sluice environment which can cause a dedicated flood area (or detention basin) to gradually fill up. Figure 2.15 shows a satellite image in which the flood area is outlined in purple and Figure 2.13 shows an image of the actual flood area.



FIGURE 2.9: Station K08_012 - local monitoring system of river parameters

2. SITE DESCRIPTION

The monitoring system of station K08_012 is shown on Figure 2.9. The close-up shows more details of all the parameters being measured, projected on a diagram of the sluice layout. This diagram can be accessed by VMM operators remotely so monitoring the parameters is possible from anywhere. Cameras are also placed around the site, so the situation can be assessed when certain irregularities appear. Also note that this data is publicly available on “<https://www.waterinfo.be/>” [37] and used in Chapter 4.

The pneumatic valves should work automatically, but manual control by turning the dials is also possible should the system fail. They can control two different types of gates: underwater and emergency gates as shown on Figure 2.11.



FIGURE 2.10: Station K08_012 - pneumatic valves



FIGURE 2.11: Station K08_012 - gate types to control downstream water level

The water level is measured up- and downstream from the station and the underwater gates are gradually raised/lowered to reach a target water level downstream, in this case 22.5 mTAW. The unit *mTAW* is short for “tweede algemene waterpassing” (translation: “second general water level”). It is a Belgian reference for height measurements relative to the sea level. All water levels provided by the VMM make

use of this reference system [38]. Note that this target can be crossed temporarily without any issues and even without having to immediately make use of the flood area. These gates are incredibly important to prevent flooding. In case they do fail, emergency gates can be used to effectively split the river in half. This control mechanism obviously influences the possible power being generated by the Arenberg site, because both head and flow rate are influenced.

The flood area can be filled until 24.75 mTAW at which point it is completely full. This only happens in extreme weather cases, such as the floods of July 2021. A graph that shows the upstream water levels over the year 2021 clearly showing the floods was added to Appendix A.

These water levels are measured by limnigraphs placed on both sides of the river and both sides of the station. Radar waves are sent to the water surface and bounced back to the device, which can calculate the distance based off the time delay. They are prone to measuring errors if e.g. a trunk is floating on the river or insects are blocking the signal, hence the redundancy. If the measured water level on both sides of the river is significantly different, one of the measurements is probably incorrect. One of the limnographs at the station is shown on Figure 2.12.



FIGURE 2.12: Station K08_012 - limnigraph used to measure water levels

2.3.2 Sediment control

Not only weather conditions can cause flooding in the city, but structures like trash racks can clog up with e.g. sand causing the water level to rise as well. Regular maintenance can overcome this, but leads to extra costs and manpower. However, this does not eliminate the possible erosion caused by sediment in combination with high flow rates. A more cost-effective method is to install a sediment trap upstream from the city. By making the river wider and deeper only at a certain point, the flow velocity naturally decreases there and the water releases sediment that sinks

2. SITE DESCRIPTION

to the bottom. This principle is used just downstream of the station as shown on Figure 2.14. The trap forms an island of sediment which is removed by a dredger boat after a certain time period.



FIGURE 2.13: Station K08_012 - upstream flood area [39]



FIGURE 2.14: Station K08_012 - downstream sediment trap [40]

2.4 KU Leuven study

A preliminary study was performed in 2014 by the KU Leuven in cooperation with the VMM to assess the feasibility of green energy production by the mill [39]. The main focus was the effects on the ecosystem should the water level just upstream from the Arenberg site be restored to the level that was set when the wheels were still in use.

2.4.1 Water level control

The former maximum water level at the mill site was set to 23.29 mTAW when water level control was still allowed at the site, which is much higher than the current target of 22.5 mTAW at the Egenhoven station 1 km upstream of the Arenberg site. Restoring this target would create a head of maximum 3.04 m, as the target water level at the Volmolen station is equal to 20.25 mTAW. This is an overestimation as the actual head should be measured just downstream of the site, instead of 1 km further. Even though this is an overestimation, it is obvious the head would increase significantly. Figure 2.15 clarifies that the effectiveness of the Egenhoven control station would decrease heavily in that case. The river is marked green and the flood area is outlined in purple. The zones marked in blue are below the former target and would therefore be underwater. An environmental impact report would be necessary to map all the effects and the possible remedies to overcome these effects, which would cost €200,000 - 250,000 (in 2014).



FIGURE 2.15: Arenberg site - zones influenced by former target water level [39]

2.4.2 Sediment control

The overall flow velocity would decrease by a water level raise, causing the sediment trap to disappear. This leads to, among other things, extra maintenance cost downstream. The exact cost is difficult to estimate.

2.4.3 Fish migration

Since the Dyle harbours about 25 fish species, some of which move upstream, a head of over 1 m makes natural fish migration impossible. It is therefore imperative to construct a fish ladder. These structures bypass the head and increase the water level step by step so that fish are still able to swim upstream. A cost of €400,000 - 700,000 (in 2014) is estimated according to the study.

2.5 Conclusion

An elaborate site description was given in this chapter. The mill site was characterised and possible improvements in terms of power generation were proposed. Next, the working mechanisms of the control by the VMM on (publicly available) river parameters was explained thoroughly. The reason that the site is described in such detail is twofold. First, the control of the water level influences the mill site directly. Having better knowledge of the system allows for more insight into the exact effects on the water wheels. Second, it should make clear to the reader why the mill site has to be studied as is. If the water level at the site is raised, all sorts of problems arise. The most important being that the entire ecosystem is more susceptible to flooding with potentially disastrous consequences. Now that the site is well-defined, the next chapter discusses the rotational speed of the Arenberg watermill in the pursuit of characterising the electricity generation capabilities.

Chapter 3

Rotational speed

The rotational speed ν of the water wheels is measured for three reasons. First, it is a necessary parameter to determine the power production as seen in Section 1.1.3. Second, the publicly available river data can be used to make a model that describes the relationship between the river parameter(s) and the rotational speed as discussed in Chapter 4. Finally, if the torque/speed curve of the water wheels is characterised, the torque (and thus inherently the power) can be derived from ν as will be discussed in Chapters 5 and 6.

This chapter starts by explaining the most common way of measuring ν and the theory behind it. This is followed by the actual implementation of this measurement. Next, the gathered data is curated, the process is described and the results are discussed. Finally, an issue causing inconsistent rotation is identified and a possible solution to the cause is proposed.

3.1 Theory

This section describes the theory behind the most commonly used method of measuring ν and identifies why it is not suitable for this research. This method is measuring the rotational speed of a spinning machine by using a commercially available digital tachometer. A lot of variations exist (optical, inductive, magnetic, etc.), but the main principle remains the same. Equally spaced marks on a rotating shaft are detected and generate a pulse. Every pulse is counted and the mean velocity over a time unit can be calculated [41]. Tachometers can be bought off the market, but a few problems occur. First, most tachometers are rated for higher rotational speeds and are thus not suited for this setup as water wheels turn slowly. The accuracy would be low. Second, most tachometers do not have the ability to log data over long time periods. Even if they could, the absence of a timestamp would render the data useless for the goal that is trying to be achieved. Finding a model that characterises ν in function of the river parameters would require alignment in time between the data. Finally, these devices can become expensive especially considering the needed functionality. A solution to these shortcomings is proposed in the next section.

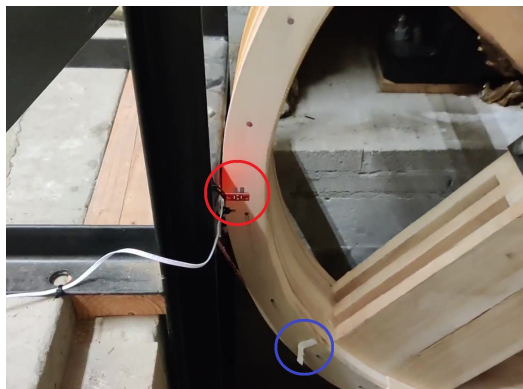
3.2 Practical implementation: custom tachometer

A custom tachometer is designed and built using inexpensive and readily available components to overcome the shortcomings of tachometers available on the market. It should be able to log data over a long time period, include a timestamp for every log and be accurate in both the measurement and the recorded time. The working principle and the installation of the module is discussed in this section.

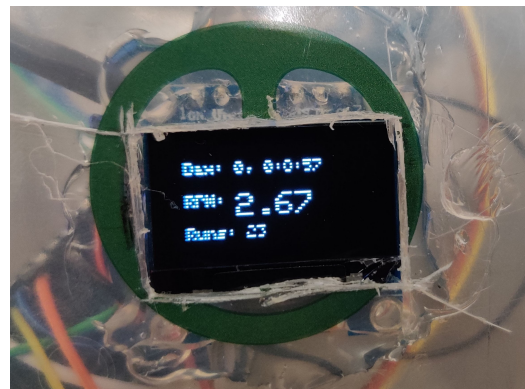
A few hardware components are needed to create a tachometer that can log timestamp and ν data over a long time period:

- Arduino MKR Zero: microcontroller that runs custom tachometer code.
- Optical switch: sets pin high/low based on detection of a light beam.
- RTC module: real-time clock used for accurate timestamping.
- OLED screen: instant visual feedback of the measured data.
- SD card: used to store the data.

A schematic of the hardware connection is added in Appendix B. The working principle is very simple. A trigger object (in this case a piece of plastic) is attached to the wooden wheel and aligned with the optical switch. If the object passes through the switch, a light beam is interrupted. Figure 3.1a clarifies this process. The switch momentarily sets a pin on the Arduino to high and a timer starts running. The next switch trigger stops, logs and resets the timer so the process can start again. The actual ν (in r/min) is found by dividing 60 s by the timer result and is displayed on the OLED screen so it can instantly be inspected as shown on Figure 3.1b.



(A) Switch (red) and trigger object (blue)



(B) Visual feedback ν

FIGURE 3.1: Custom tachometer - v1 - installation

3. ROTATIONAL SPEED

Along with the timer results, a timestamp in Unix form is logged. The Unix representation is a single number that represents the number of seconds passed since midnight 01/01/1970 UTC [42], which makes it easier to handle in code. The timestamp is tracked by the RTC module, which has two major advantages over the internal clock: it takes the ambient temperature into account making it much more accurate, and it has a backup power supply should the main power fail [43]. This prevents drift or time resets from skewing the alignment with the river data. Both the timestamp and the timer result is logged to a single row in a .csv file on the SD card, so the data can easily be processed further.

Only one trigger object is used, so this method is not able to intercept any transients. Because rivers tend to be relatively slow-changing in nature, this was not expected to be an issue. However, there is a different effect that makes the rotational speed vary over one single rotation which is discussed in Section 3.5. This means the rotational speed ν used in this thesis generally represents the mean of the no-load speeds in one single rotation.

The attentive reader might wonder why an offline logging system was used instead of e.g. an online web app. This would be much more accessible and simpler/cheaper in hardware as the RTC module and SD card would not be needed. The reason for this is simple: there was no WiFi network available for a microcontroller to connect to. As of summer 2022, this is possible and a new implementation is discussed in Chapter 7.

3.3 Data curation

The logged data cannot be used in raw form and should be curated by performing multiple operations on it. A flowchart is used to better keep track of these curation operations and other processes on the data throughout this chapter and the next. Every section only contains the relevant part of the flowchart. The relevant parts for this section are shown on Figure 3.2 with parallelograms representing the data and the rectangles representing the operations. The entire flowchart can be found in Appendix C.2.

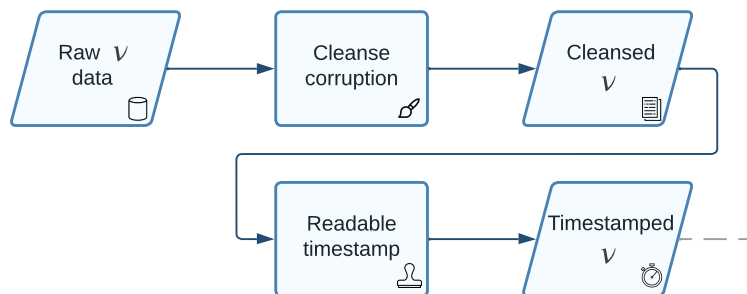


FIGURE 3.2: Modelling flowchart - data curation rotational speed

Cleanse corruption

Raw data often contains some corrupted values, as seen on Figure 3.3 that is the case here too.

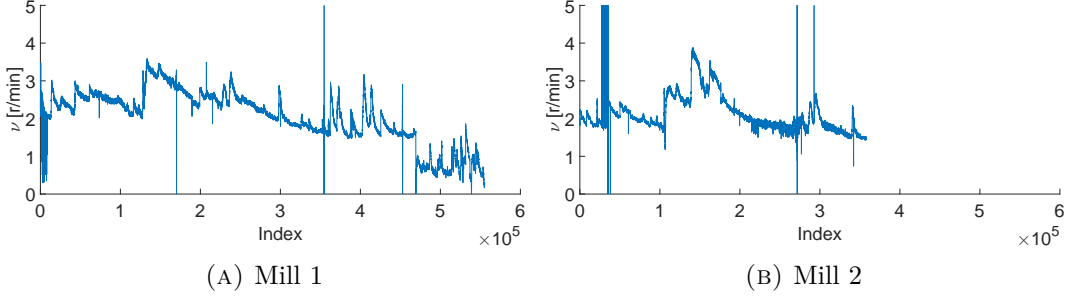


FIGURE 3.3: Rotational speed - raw data

The raw data contains two types of corruption: sudden peaks and chunks of unrealistically high, constant values. These corrupted values are easy to find and remove due to their nature relative to neighbouring values, yielding cleansed data as seen on Figure 3.4.

Readable timestamp

As mentioned in the previous section, the ν data on the SD card is logged together with a Unix timestamp. Converting that into a readable 'human' timestamp whilst taking the daylight saving times into account yields Figure 3.4. This makes it easier to interpret the evolution of ν in time.

3.4 Results

Over 500,000 data points for mill 1 and close to 340,000 data points for mill 2 were gathered between December 2021 and September 2022. Mill 1 has more data, because mill 2 was used to determine the torque/speed characteristic which would influence ν_2 . Large gaps do occur due to a faulty power adapter, but more than enough data was gathered to make statistically relevant claims. Visual inspection shows the same trends for both mills, with ν_1 consistently higher than ν_2 . This chapter does not discuss any relations between ν_1 and ν_2 themselves or between ν and other river parameters. This is handled in Chapter 4.

Note that ν_1 is separated into two time periods: 07/12/21 - 24/06/22 and 12/07/22 - 25/09/22. This is because the summer of 2022 was the driest ever recorded in Belgium [44]. In combination with extreme temperatures this caused drastic change in river parameters. Section 4.2.2 discusses this in detail and characterises the change. The distinction in time periods will consistently be made. Also note that ν_2 is measured exclusively during the first time period, even though the exact dates differ slightly.

3. ROTATIONAL SPEED

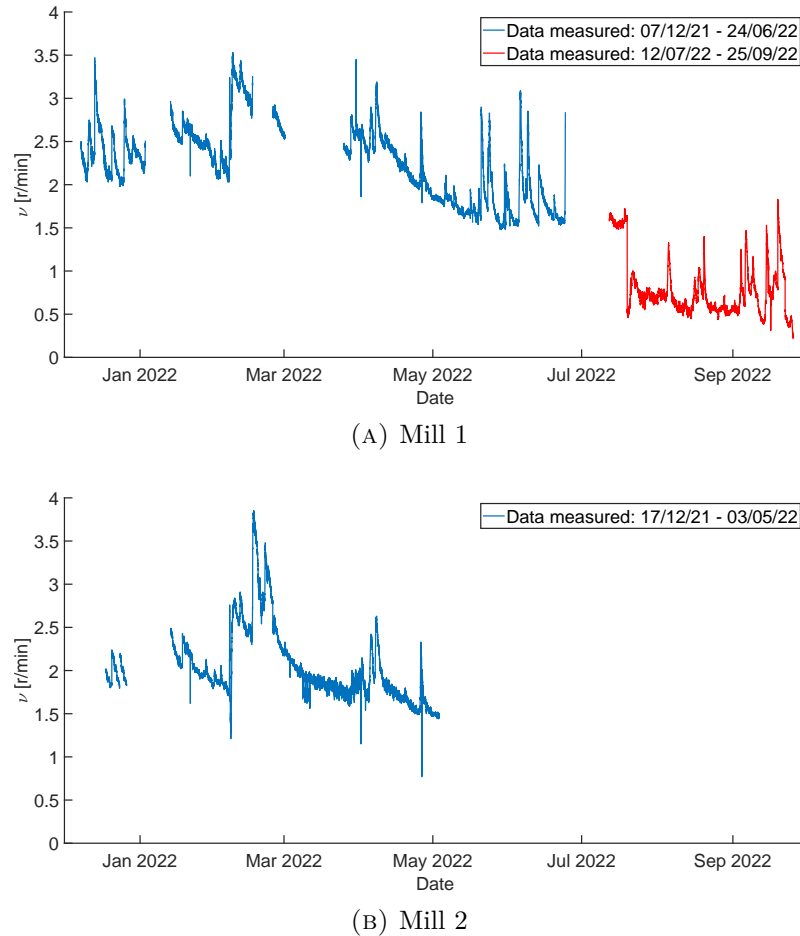


FIGURE 3.4: Rotational speed - timestamped

Both mills show a fairly large variation ranging between 0.5 to 4 r/min. The cause of this variation is logically due to varying river parameters and is discussed in Chapter 4. During the first measurement period, the average ν_1 was 2.24 r/min and ν_2 averaged at 2.13 r/min. Note that these values should not be compared here as each mill has gaps at different points in time. During the second measurement period, only mill 1 was measured and averaged at a ν_1 of 0.79 r/min. This is significantly lower than the first measurement period and the reason for this will also be discussed in Section 4.2.2

3.5 Inconsistent rotation

As explained in Section 3.2, ν is determined by the time needed for one full rotation and can therefore not detect any transients in that rotation. During the torque measurements performed in Chapter 5, it became clear that the momentary ν is changing constantly over one rotation. This is true for both mills and seems to

happen consistently. Several hypotheses are proposed and tested.

First, there might be some kind of interaction between the mills. This was quickly discarded by putting one of the mills to a halt to see the effect on the other. This made no difference to the inconsistency and was therefore not the origin of the issue. Second, the water might flow to the wheels in an inconsistent manner. This hypothesis is hard to prove and most likely needs complicated fluid dynamic analysis and extra measuring devices. However, confirming another hypothesis would remove the need for this.

Finally, the water wheels might be poorly balanced, meaning the weight distribution is not even. This would cause a shift in centre of gravity, away from the centre of rotation. This rotating imbalance would cause clear and consistent oscillatory behaviour in ν with a period equal to the time it takes for a single rotation.

Figure 3.5 shows a simplified visualisation of rotational imbalance to better understand what is potentially happening. Imagine an imbalanced water wheel is turning clockwise, with the centre of gravity placed in the solid red triangle and the centre of rotation in the light blue circle. At this position the wheel will turn faster, because gravity pulls down on it. The opposite occurs 180° further, when the centre of gravity is at the dotted line. The wheel now has to pull up its centre of gravity, causing it to turn more slowly. This means half of the time the actual ν is linearly increasing, the other half it's linearly decreasing (as the acceleration is constant and equal to g). A balanced water wheel would have its centre of gravity coincide with its centre of rotation or visually speaking: the red triangle would coincide with the blue circle.

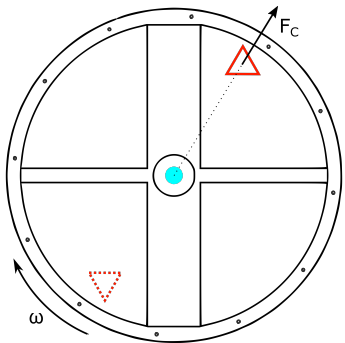


FIGURE 3.5: Rotating object imbalance visualisation

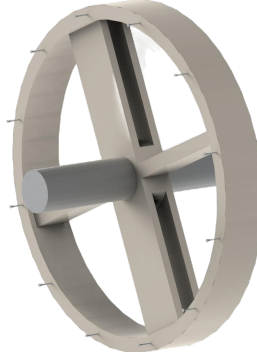


FIGURE 3.6: Arenberg water wheel - equally spaced trigger points

A total of twelve equally spaced measuring points are placed on mill 2 as shown on Figure 3.6 to properly analyse this effect. Unfortunately the optical switch was malfunctioning, causing measuring points to sometimes be undetected. The raw result is shown on Figure 3.7a: a band of tangled values appear instead of getting twelve different ν curves. There are time periods where some measuring points are detected correctly and consistently, but the data has to be selected and shifted

3. ROTATIONAL SPEED

around first. The untangled result is shown on Figure 3.7b. Figure 3.7c shows the longest separated time period, with eight detected measuring points. This data was transformed to show the measure points chronologically on Figure 3.7d. Note that every subfigure zooms in further on the data to create a better oversight.

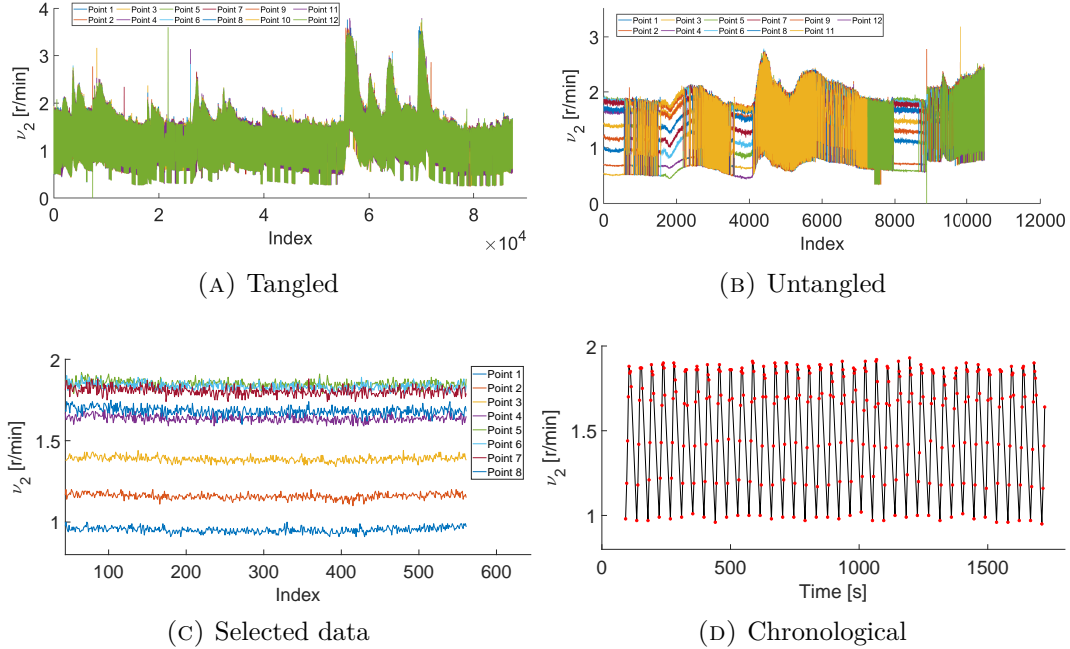


FIGURE 3.7: Rotational speed - measurements inconsistent rotation

Figure 3.7 clearly confirms the rotation imbalance hypothesis as consistent oscillatory behaviour is found in a single rotation. This imbalance can have drastic consequences from both a maintenance/lifetime and an operational point of view. The bearings and the supporting structures need more maintenance and wear more quickly due to the created centrifugal force and resulting vibration [45]. This vibration is a source of efficiency loss as well, generating heat instead of mechanical power and can be detrimental to gearboxes that might be placed in the future. From an electrical point of view, the pulsation causes fluctuation in voltage level and frequency. This can make it harder if not impossible to establish a grid connection should certain thresholds be crossed.

There are multiple possible causes for the imbalance, the main ones being built quality and corrosion/wear [46]. The most likely cause is built quality as both wheels are designed to be identical and show the same effect. The production process might have introduced a few faults e.g. a certain eccentricity, the steel frames may differ in weight... Corrosion seems less likely as the wheels were installed relatively recent and there is no visual sign of any rust form on the outside. A solution would be to add mass at certain locations around the wheel or remove mass at the opposite site

of those locations. Finding these locations is considered out of scope, as the site is studied as is.

3.6 Conclusion

This chapter proposed and implemented a method to log the rotational speed ν of the water wheels. A custom tachometer was constructed that fulfils all the needed specifications: accurate logging of both data and timestamp. A vast amount of data was gathered for both mills individually, which was then curated to remove corrupted values and add readable timestamps.

Furthermore, it was discovered that the water wheels do not turn at a consistent rate in one rotation, for which multiple hypotheses were put forward. The final cause was determined to be a rotational imbalance. In turn, possible causes for this imbalance were put forward and a possible solution was proposed.

The next chapter discusses more operations performed on the curated ν data to yield a model that is able to estimate the rotational speed in function of measured river parameters at the VMM control stations.

Chapter 4

Modelling

Now the rotational speed data is collected and organized, the river parameter data provided by the VMM can be used to characterise ν in function of these parameters. An attempt is made at modelling ν using head, flow rate and water level data. First both data resources are further curated, so they can be compared in a meaningful way. Next, they are aligned in time and the influence of the different river parameters on ν is investigated. A separate model for ν that is valid under certain conditions is proposed for both mills. Finally, the use cases for this model are discussed.

4.1 Data curation

4.1.1 River parameters

As discussed in Section 2.3, river parameter data from the VMM is publicly available and used to model the rotational speed. Although the VMM is constantly monitoring the parameters in real-time, the available data is only published every 15 minutes. The VMM provides a readable timestamp and quality codes with every data entry. Two different types of river parameters are used: the flow rate Q and the water level h .

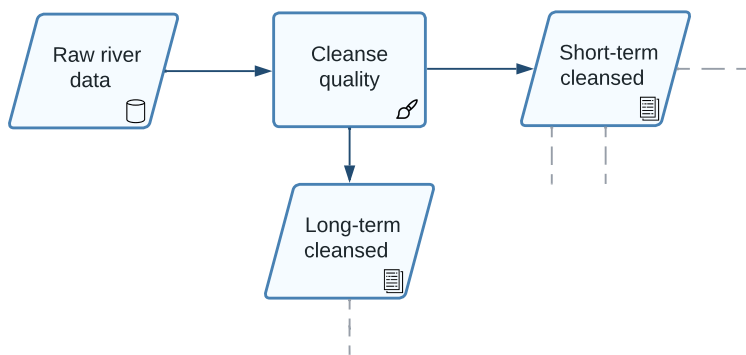


FIGURE 4.1: Modelling flowchart - river parameter processing

The river data needs to be curated as well, which is easily done by using the quality codes. There are nine different qualities, for which the codes are listed in Appendix C.1. Only the data entries marked “Excellent” and “Good” are used to get the best possible model, the rest is deleted. The relevant parts of the flowchart from Appendix C.2 are listed in each step again, as shown on Figure 4.1. There are two outputs (and in reality two inputs, omitted for conciseness): the long-term data dating back to 2006 and the short-term data that overlaps with the measuring period of ν .

4.1.2 Rotational speed

The timestamped ν contains all the logged data. To find a model, the only data needed is the ν at every 15-minute interval. This is because the river parameters are also only available every 15 minutes. Note that the data is only logged after a full rotation completes. If $\nu < 1 \text{ rad/s}$, there might not be a value at exactly every 15-minute interval. A margin of 2 minutes is allowed to include as much data as possible.

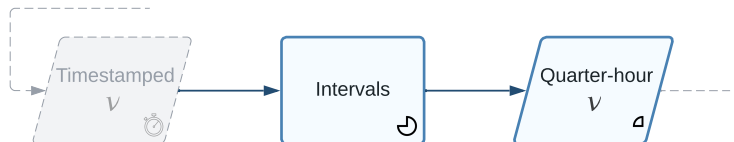


FIGURE 4.2: Modelling flowchart - quarter-hour ν intervals

4.2 Data alignment

Both river and ν data are now available at 15-minute intervals. Note that both data resources also have gaps due to corrupted values or unrecorded time periods. Every value needs to be matched according to their corresponding timestamp, to get relevant data pairs. This yields ν in terms of the river parameter data. Because not all river parameters are available at every station, a relationship between Q and h is found to indicate they have the same influence on the rotational speed under certain conditions. An oversight of these operations is shown on Figure 4.3.

4.2.1 Head

As discussed in Section 1.1.1, undershot wheels are mainly driven by kinetic energy. The influence of the head should therefore be negligible. The difference of the water levels from the up- (Egenhoven) and downstream (Volmolen) stations is calculated to investigate this hypothesis. Note that this difference is not equal in value to the head across the watermill, but a 1-on-1 relationship between the actual head and the water level difference is assumed. This is reasonable as there is no distributary (river sidestream) or water level control between the measuring stations. Figure 4.4 confirms the hypothesis. Because of the water control by the VMM, the water

4. MODELLING

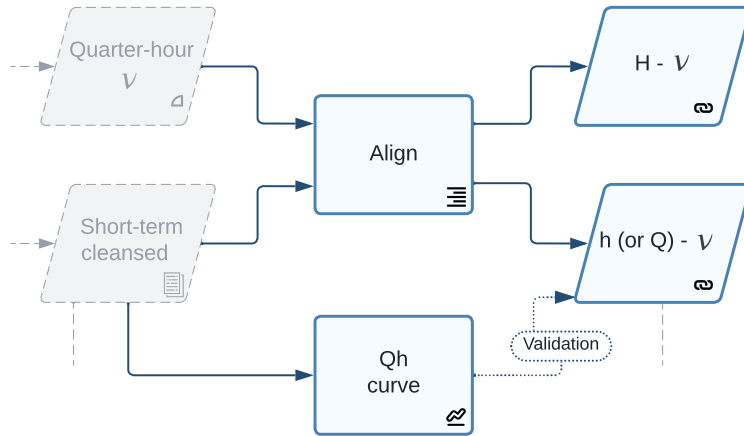


FIGURE 4.3: Modelling flowchart - data alignment

level difference is kept constant most of the time at around 2.25 m, but a large variation in ν is shown, concluding that the influence must be due to another river parameter. Note that there is some variation in the head in the summer of 2022 shown on Figure 4.4a due to the aforementioned drought and drastic change in river parameters.

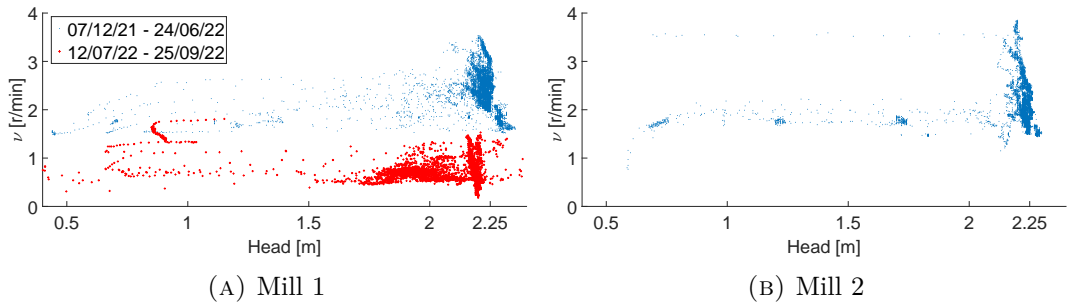


FIGURE 4.4: Rotational speed - function of head - Volmolen-Egenhoven

4.2.2 $Q(h)$ curve

Ideally, the next river parameter to align with is the flow rate Q . It is an indication of the kinetic energy contained in the water and thus presumably the best parameter to model with. Unfortunately, the closest stations only provide water level data, while the first station that does provide flow rate data is located 8 km upstream from the mills in Sint-Joris-Weert (SJW). Its exact location is shown in Appendix A.3. This data cannot directly be used as there are control stations and distributaries in between SJW and the mills, which can obviously have a significant influence on the flow rate. Figure 4.5 confirms this statement, showing no clear relationship between Q and ν . It can however be used to estimate general tendencies of the river.

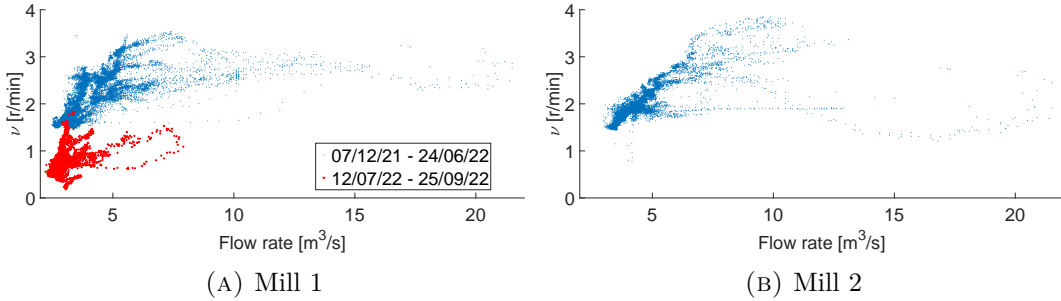
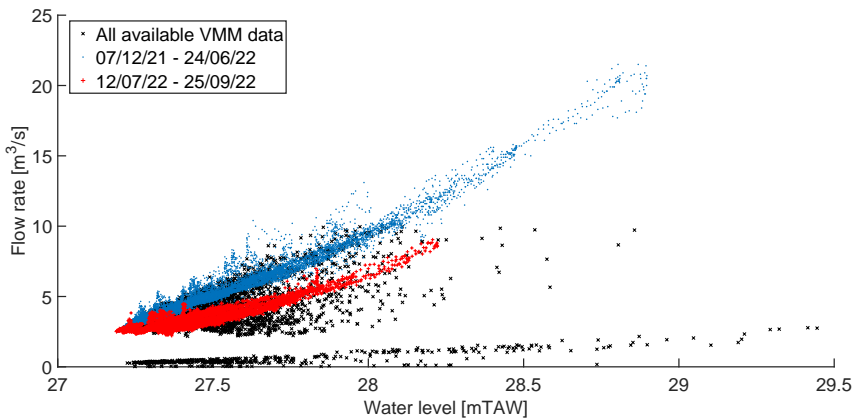


FIGURE 4.5: Rotational speed - function of flow rate - SJW

Although the water level of a river shows no obvious connection to ν (unlike H and Q through Equation 1.3), it is still possible to use the water level data from the closer stations. This is because river flow rates can often be characterised in function of the water levels by a stage-discharge relationship or $Q(h)$ curve [47]. A $Q(h)$ curve thus makes it possible to indirectly get the flow rate by measuring the water level. Note that this is a dynamic curve in the sense that this relationship can change over time due to e.g. drought, geometric changes in the channel bed, etc.

All available $Q(h)$ data points of the Dyle at the SJW station are shown on Figure 4.6. Two distinct curves are visible each belonging to a separate time period. Note that these time periods match the time period distinction made in ν_1 as discussed in Section 3.4 and that this is no accident. The curves characterise the change in river parameters due to extreme temperatures and drought. The reason for separating the time periods should now become clear: each time period belongs to one static $Q(h)$ curve and should thus be handled separately.


 FIGURE 4.6: Relationship between flow rate and water level $Q(h)$ - SJW

For simplicity, the second time period (12/07/22 - 25/09/22) is omitted from now on. The operations described in next sections can however be repeated on this time period as well, leading to similar results and conclusions. Note that the flow rates during this time period are lower for the same water level, which explains the significant

4. MODELLING

drop in average ν seen in Section 3.4. The first time period (07/12/21 - 24/06/22) contains more than enough data for both mills and is therefore chosen for further research. A reasonable assumption is made that the $Q(h)$ curve at the closer stations is static when the $Q(h)$ curve at the SJW station is static. Therefore, there must be a 1-on-1 relationship between flow rate and water level during the first time period. This means h can be used as an indication for the kinetic energy contained in the water and thus can be considered a good river parameter to model with.

This assumption and the dynamic nature of the $Q(h)$ curves are the largest caveats of the model that is being built. First, it is perfectly possible there is a large change in between SJW and the closer stations in e.g. the channel bed that causes a visible shift in the $Q(h)$ curve at the closer stations, but not in SJW. Second, the dynamic nature of $Q(h)$ creates the need for multiple models, one for each $Q(h)$ curve. A solution for these shortcomings would be a model that is completely independent of the $Q(h)$ curve and characterises $\nu(Q)$ directly instead of indirectly. However, direct flow rate measurements are expensive to perform [47] and the VMM is not likely to install extra hardware at the closer stations as the SJW station is still relatively close. If this should ever happen, it would be beneficial to redo the models.

4.2.3 Water level (or flow rate)

The water level measured just downstream of the Egenhoven station (and thus upstream of the mills) or just upstream of the Volmolen station (and thus downstream of the mills) is logically the best indication of the flow rate at the mills. Both are aligned with ν and the data showing the most obvious relationship is selected. The Egenhoven data in Figure 4.7 does demonstrate a discernible relationship between ν and h . There seem to be multiple curves present in the figure, indicating there must be another parameter influencing ν . This parameter is discussed in the next section. The Volmolen data is included in Appendix C.3, but shows this relationship to a lesser extent.

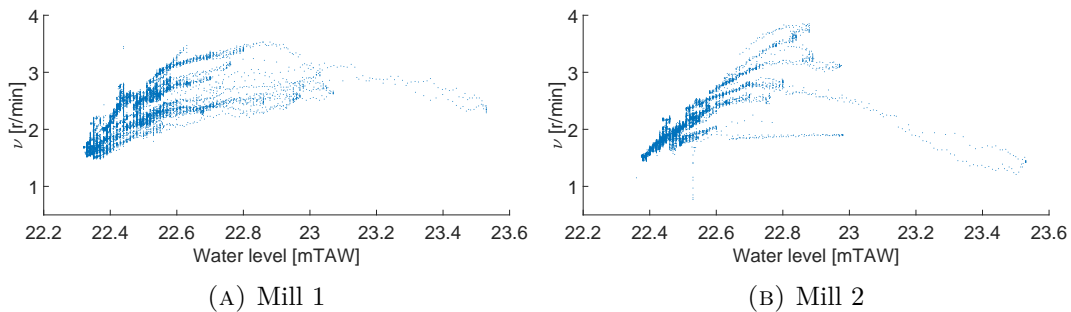


FIGURE 4.7: Rotational speed - function of water level - Egenhoven

4.3 Regression analysis

Now that the parameter showing the main influence on ν is determined to be the flow rate (replaced by h as it is the only available parameter) and river data is aligned with ν , it is possible to characterise a $\nu(h)$ curve using regression analysis. Before fitting a curve, the aligned data has to be placed in separate bins first to account for the second parameter influencing ν . Then, the best possible model with the data available can be created using the bins containing most data.

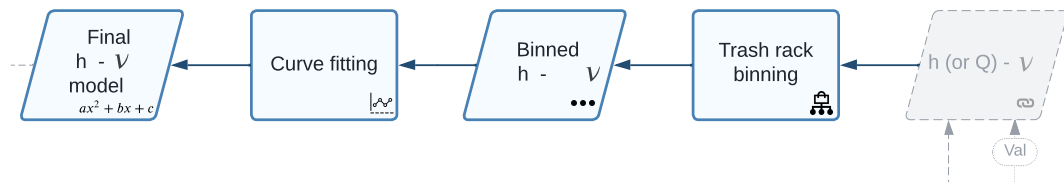


FIGURE 4.8: Modelling flowchart - regression analysis

4.3.1 Data binning

The second parameter is assumed to be the amount of debris built up by the trash rack: the more debris, the less water is able to get to the water wheels causing a change in ν . The different curves do not gradually merge from one to the other, but have a rather abrupt gap between them. This is most visible for mill 2 on Figure 4.7b and indicates there must have been an abrupt change in the environment.

Mill 1 does show, to some degree, a more gradual transition between curves. This is most likely due to the placement of the wheels and the trash rack. The trash rack is placed in front of the mills under an angle as shown on Figure 4.9, so that debris can still flow away with the water that does not flow towards the mills. Mill 1 is positioned on the left side relative to the figure where it is more likely for debris to pile up gradually. This is clearly shown on the figure as well, with significantly more branches on the left side as opposed to the right. Smaller branches are less likely to get caught on the right side as they can easily be dragged along with the current. If something does get caught, it is more likely to be a bigger object that is less easily dragged along. This big object would have a more significant and abrupt influence on ν , explaining the more abrupt jumps between curves for mill 2.



FIGURE 4.9: Arenberg site - trash rack with built-up debris

4. MODELLING

There is no way to quantify or measure the amount of built-up debris, which makes it difficult to create an accurate model. A solution would be to place an automatic trash rack cleaner, clear the debris manually on a more regular basis or installing a more coarse trash rack allowing for some debris to enter the system. An attempt is made however, by creating multiple bins each representing a “built-up debris stage” and assigning every data point to a bin. This yields Figure 4.10 with the amount of data points in each bin shown between parentheses in the legend. The outliers of mill 2 are most likely due to measurements of the limnigraph of a floating object on the river as described in Section 2.3.

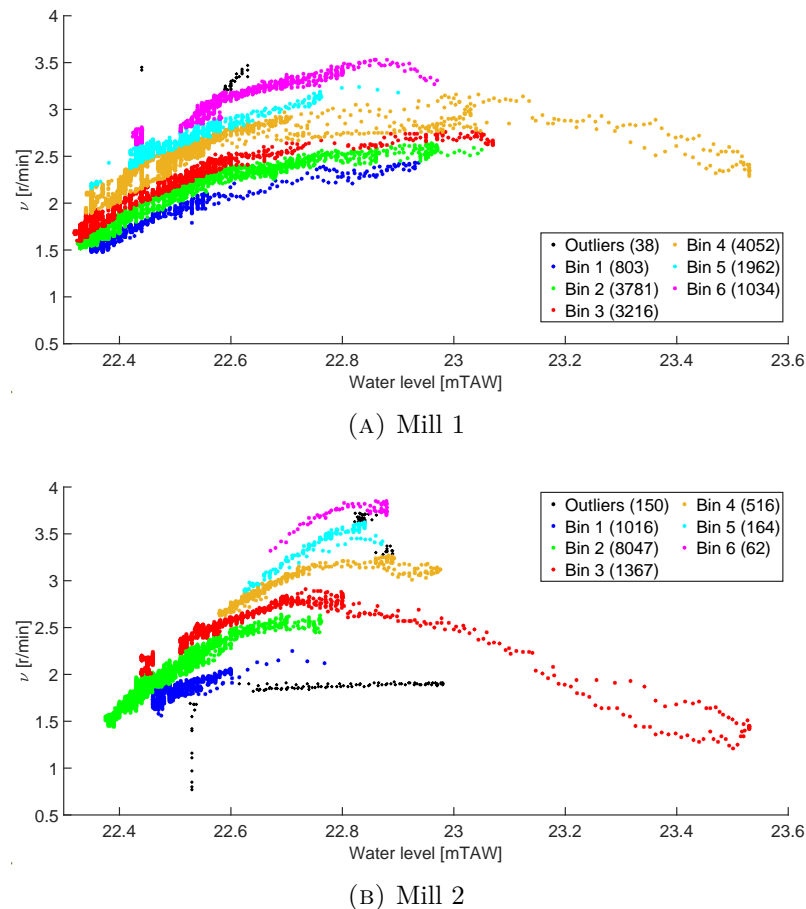


FIGURE 4.10: Rotational speed - function of water level - data bins

Mill 2 has over 70% of its data points in bin 2, further strengthening the hypothesis of the debris build-up having less effect here because of the mill placement relative to the trash rack. Because most data points are concentrated in one bin and there is abrupt change between bins, there must be occasional and abrupt change causing it. Mill 1 has most data points spread over bins 2, 3 and 4 also reaffirming the idea that debris is gradually build up in this case, making ν more sensitive to debris.

The fact that the mills experience a difference in debris build-up is also one of the reasons why the rotational speed profile of both mills is different. However, the fact that mill 1 is consistently turning at higher speeds is now counterintuitive. Quicker, more consistent debris build up should result in lower ν . Therefore, there must be another cause e.g. channel bed inconsistencies, better lubricated axle, etc. Also note that mill 1 is closer to the instant drop present at the site, causing a consistently higher head. Although the head as a whole is not considered as a main influencing factor for the current setup, it can still contribute to the observed difference.

Another influencing parameter might be the sediment trap upstream. More sediment causes more momentum transfer from the water to the sediment and thus lower flow rates. Because the trap is only cleared once every few years and forms slowly, this hypothesis cannot be tested for now.

4.3.2 Curve fitting

Now that every data point has been assigned to a bin, a few options to fit a curve are available. First, it is possible to fit a curve to every separate bin and thus characterise them individually. However, there is no way to use these models in any meaningful way as long as the debris cannot be quantified. Therefore, a less accurate but more meaningful option is chosen: combining bins containing the most data and fitting a curve to the resulting bin. The excluded bins are considered outliers, which is not unreasonable as at least 70% of the data is included in the final models and the trash rack would most likely be cleaned more often should electricity generation be feasible.

Before fitting a curve, it is necessary to determine the regression type (linear, quadratic, cubic, etc.). In general, all data bins seem to show a quadratic relationship between ν and h , with ν_1 reaching a maximum around 23 mTAW and ν_2 reaching a maximum around 22.8 mTAW. If the water level was a perfect replacement for the flow rate, such a relationship would be counterintuitive as higher flow rates would equal higher hydraulic power and therefore higher ν . However, the water level itself does have an influence at some point. Because of the unfavourable blade angle described in Section 2.2.1, a higher water level means higher resistance as more water has to be pushed upwards. At some point, this resistance becomes more significant than the increase in flow rate and thus cause a decrease in ν . Therefore, a concave quadratic relationship is assumed and fitted to the data for both mills.

Note that the difference in water level for the maximum point can be attributed to the fact that mill 1 is closer to the drop at the site. The channel bed is slanted at a slight angle, causing mill 1 to appear higher than mill 2 relative to the main river. This makes mill 1 experience the overtaking of the resistance effect at a slightly higher water level than mill 2.

Mill 1

Bins 2, 3 and 4 contain around 75% of the data points for mill 1 and are combined into one bin. The quadratic fit is shown in Figure 4.11. The resulting equation that characterises the rotational speed ν_1 in function of the water level at the Egenhoven station h is as follows:

$$\nu_1(h) = -3.12 h^2 + 143.28 h - 1641.55 \quad (4.1)$$

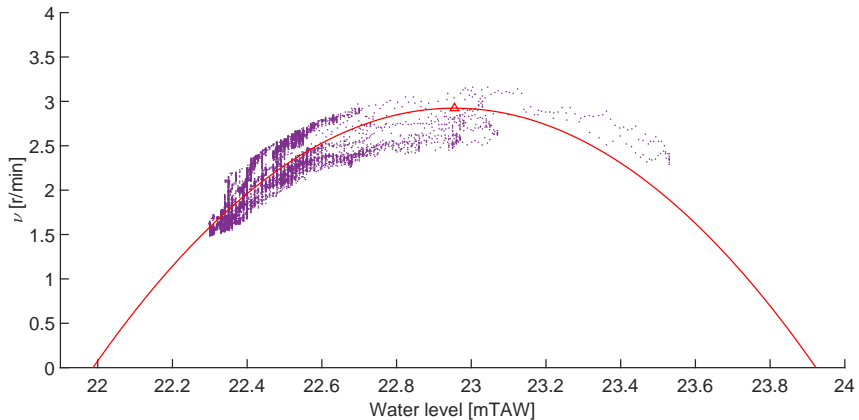


FIGURE 4.11: Rotational speed - mill 1 - function of water level - final model

The fitted curve has an R^2 (coefficient of determination) value of 0.76. This suggests that the curve fits the data reasonably well and the underlying relationship is captured. However, it is important to note that R^2 is only one measure of the goodness of fit of a model, and other factors e.g. residuals should also be considered when evaluating the quality of the fit. These residuals are added in Appendix C.3 and show no discernible pattern. This is another indication that the chosen quadratic regression is a good choice. R^2 and residuals are used throughout this research to assess the quality of a fitted curve.

Mill 2

Mill 2 is more straightforward as bin 2 already contains most of the data and therefore no bins have to be combined. The quadratic fit is shown on Figure 4.12. This fit logically has a higher R^2 of 0.96 and also no discernible pattern in the residuals (see Appendix C.3). The resulting equation that characterises the rotational speed ν_2 in function of the water level at the Egenhoven station h is as follows:

$$\nu_2(h) = -7.24 h^2 + 329.73 h - 3751.05 \quad (4.2)$$

Note that mill 2 is more sensitive to changes in water level as the curve is more narrow than the fit of mill 1. This is most likely due to the fact that mill 1 experiences more influence from the debris build-up, as discussed before.

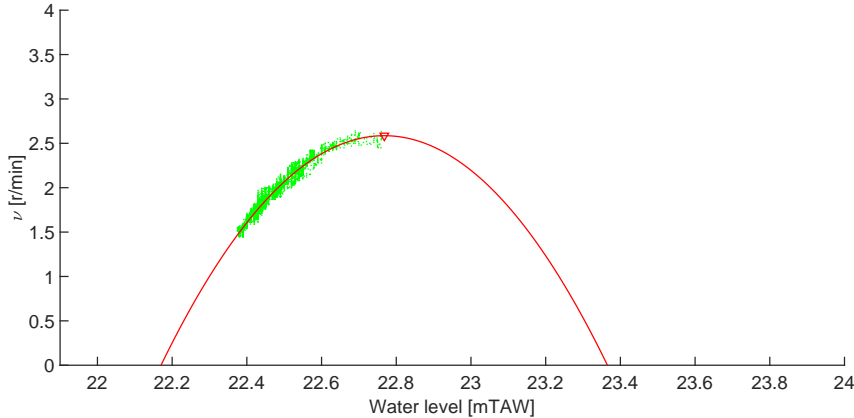


FIGURE 4.12: Rotational speed - mill 2 - function of water level - final model

4.4 Model usage

Now that the final $\nu(h)$ models for both mills are known, it is possible to use them for looking at the past or the future and estimating ν by using past or forecasted h measurements. The model is only valid under certain conditions, which should be checked before use.

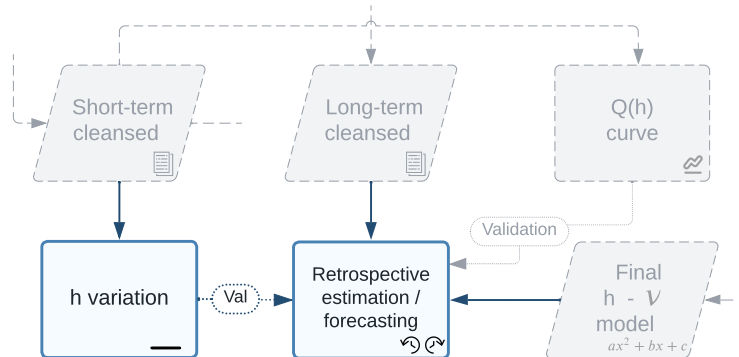


FIGURE 4.13: Modelling flowchart - retrospective estimation

4.4.1 Retrospective estimation

Long-term water level data at the Egenhoven station is available dating back to 2006 and can thus be used as an input of the $\nu(h)$ models. There are two considerations to keep in mind when performing this retrospective estimation. First, only a single measurement for each day is available in the long term data. Second, the $Q(h)$ curve is dynamic and should therefore be evaluated for every time period that is being estimated.

4. MODELLING

Daily variation in water levels

Because there is only one measurement available for each day in the long-term data, it is important to check how the water level varies in a single day. If there is a large variation, the single measurement cannot be used as a representative value for the entire day. The quarter-hour short-term data between 27/10/2021 and 30/11/2022 (400 days) is used to investigate this variation. The standard deviation in h of a single day can be used to quantify the daily variation, but does not provide any information on the general variation. This is because these standard deviations cannot be compared between multiple days as every day has a different mean. A more meaningful statistic measure is the coefficient of variation (CV), often used to compare the variability of different datasets [48]. In this case, each day can be handled as a separate dataset. The CV of a single day can be calculated by:

$$CV_h = \frac{\sigma_h}{\mu_h} \quad (4.3)$$

σ_h represents the standard deviation and μ_h represents the mean, both of the water level in a day. The standard deviation in a day is calculated by:

$$\sigma_h = \sqrt{\frac{\sum_{i=1}^N (h_i - \mu_h)^2}{N}} \quad (4.4)$$

Where N represents the number of measurements for h in that day. These formulas allow for the individual calculation of CV_h for 400 days. The mean of these CV_h 's can then be calculated, resulting in a single number μ_{CV_h} quantifying the general variability in the water level.

For the Egenhoven station, μ_{CV_h} is equal to 0.116% indicating there is very low general variability in the water level in a single day. The long-term data can therefore be used for a retrospective estimation of ν .

$Q(h)$ curve validation

If the $Q(h)$ curve for the time period being estimated coincides with the $Q(h)$ curve between 07/12/21 - 24/06/22 of Figure 4.6, the model is considered to be valid. However, if it does not coincide (e.g. the $Q(h)$ curve during the summer of 2022) the model is invalid for that time period and no estimation can be carried out.

The validated $Q(h)$ data points are showed again in Figure 4.14a. This time a curve is fit and a band is created around this curve. This band is made to include 98% of the data points, effectively excluding outliers and therefore the best representative of the $Q(h)$ curve during the modelling time period. Note that previously the “ $Q(h)$ data points” and “ $Q(h)$ curve” were used interchangeably. From now on the $Q(h)$ curve is meant to be the band that includes 98% of the validated data points.

All available long-term $Q(h)$ data points of the Dyle at the SJW station are evaluated against this $Q(h)$ curve. The band is superimposed on the long-term data as shown on Figure 4.14b, exposing which data points and thus which time periods can be used to retrospectively estimate ν . Because only 50% of the data is situated in the band, the model is only valid half of the time. This underlines the previously discussed shortcomings of the model. This result insinuates there might be a seasonal effect, but this does not seem to be the case. A scatter plot separating $Q(h)$ data points into winter (Jan-Jun) and summer (Jul-Dec) is shown in Appendix C.3, but shows no discernible trend.

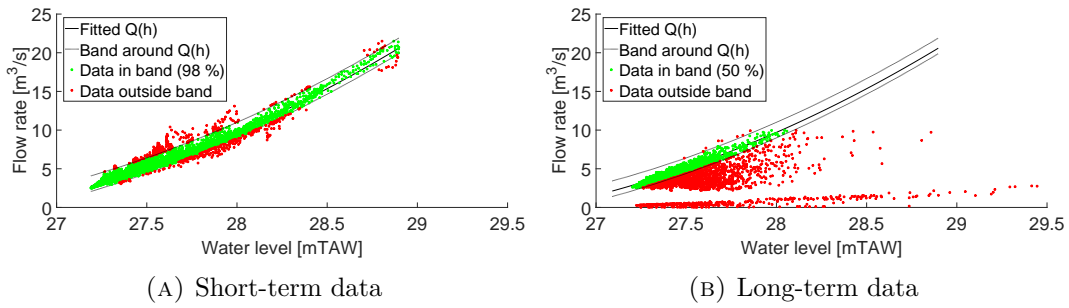


FIGURE 4.14: Band around $Q(h)$ to validate the final model - SJW

Now the time periods when the model is valid are known, it is possible to perform the retrospective estimation of ν and therefore eventually estimate the power production P_{mech} at those times using the torque/speed characteristics still to be determined in the next chapter.

4.4.2 Forecasting

The VMM provides forecasted values for the water levels 10 days in the future as shown in Appendix C.3, making it possible to use the models to forecast ν and therefore forecast the power P_{mech} using the torque/speed curves characterised in the next chapter. Note that the model validity should still be checked here too.

4.5 Conclusion

An attempt was made at modelling the rotational speed of both mills ν_1 and ν_2 in terms of river parameter data provided by the VMM. With the current available data, a robust model could be fitted that describes ν in terms of the water level h with reasonable accuracy under certain $Q(h)$ river conditions. Inaccuracies in the model predictions can largely be attributed to the unpredictability of the debris caught in the trash rack placed before the mills. If there would be more regular maintenance, a more coarse trash rack or even an automatic trash rack cleaner, it is possible to improve the accuracy by eliminating the debris build-up. With the current setup, mill 1 suffers most from the debris because of the placement relative to the trash rack, while mill 2 only suffers from seemingly larger and abrupt debris.

4. MODELLING

Should direct flow rate measurements at the Egenhoven station upstream from the mills ever become available, it is possible to make a $\nu(Q)$ model that is always valid. Otherwise, more ν measurements should be performed at different $Q(h)$ curves to get multiple models and thus more coverage in time.

The developed model can be used to perform a retrospective estimation or forecast ν , but should always be checked against the $Q(h)$ curve for validation. In combination with the torque/speed characterisation of the watermills, it is possible to perform the same estimations for the mechanical power produced by the mills P_{mech} . These torque/speed curves are characterised in the next chapter.

Chapter 5

Torque

The ultimate goal of this thesis is to determine the mechanical power P_{mech} delivered by the water wheels to assess if the electricity production is financially viable. Since last chapters gathered information on ν , the only parameter left to determine is the torque T . This chapter discusses the methods used to measure T so the torque/speed curves can be characterised.

First, the theoretical methods for torque measurements are discussed. Next, the most suitable method is selected and its practical implementation is evaluated. This is followed by the exploration of a creative way of measuring the average torque in a rotation using OCR software, necessary due to practical issues. Finally the results are discussed and two torque/speed curves are characterised.

5.1 Theory

There are different possible techniques to measure the torque of a rotating machine. This section discusses the most relevant methods before selecting the best suited one. The difficulty is that the shaft is moving during the measurement, as dynamic torque is needed to determine P_{mech} .

5.1.1 Torque transducers

Torque inherently means there is a force present on the rotating shaft, which in turn causes the shaft to deform slightly. Strain gauges are devices that deform under mechanical stress, causing their resistance to change. They can detect even the slightest strain if arranged properly, making them ideal for highly accurate torque measurements [49]. Four strain gauges can be placed on the shaft as shown on Figure 5.1 to create a torque transducer. From an electrical point of view, the strain gauges have to be arranged in a Wheatstone bridge. The change in resistance can then be detected in the form of an output voltage [50]. This change in output voltage is indirectly linked to the torque and can therefore be used to get a torque

5. TORQUE

measurement. First a known torque has to be applied so the device can be calibrated.

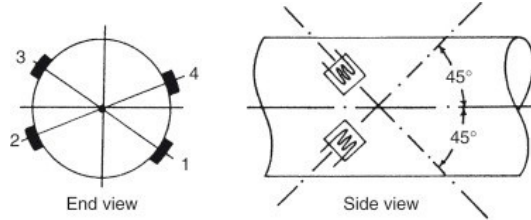


FIGURE 5.1: Theoretical method torque - torque transducer - strain gauge [51]

An advantage of this method is that the voltages (and thus torques) can accurately be constantly logged with the Arduino that is already present for rotational speed measurements.

Unfortunately, the disadvantages outweigh the advantages. The largest caveat of this method is that the placement has to be very precise, otherwise the measurements are inaccurate [51]. Furthermore, the electrical connection between the torque transducer and the voltmeter/Arduino has to be ensured while the shaft is turning to measure the dynamic torque. Therefore, slip rings are needed or a wireless connection can be established [52]. These disadvantages lead to extra costs and uncertainties, making the use of a bare torque transducer unfavourable.

5.1.2 Prony brake

The Prony brake is by far the most used form of measuring torque in similar research [11, 14, 19, 21, 26, 35, 53–56], because it's simple, inexpensive and reasonably accurate. The general principle is explained first, followed by a more applied version to the site setup.

General principle

Figure 5.2a represents a version set up in its simplest form. A rotating shaft is clamped between two wooden blocks that can be tightened by screwing them closer together. The top block is connected to a lever arm with length L , measured from the centre of the shaft. The clamp structure will start rotating along with the shaft due to the friction, until it cannot move further. Next, weights can be hung from the other end of the arm to compensate the torque performed on the clamp structure by the rotating shaft. The arm should be perfectly horizontal again, so the weights cause an equal, but opposite torque on the clamp structure. If the weights have a total mass m , the torque T produced by the shaft can be calculated with the following equations:

$$F = m \cdot g \quad (5.1a)$$

$$T = F \cdot L \quad (5.1b)$$

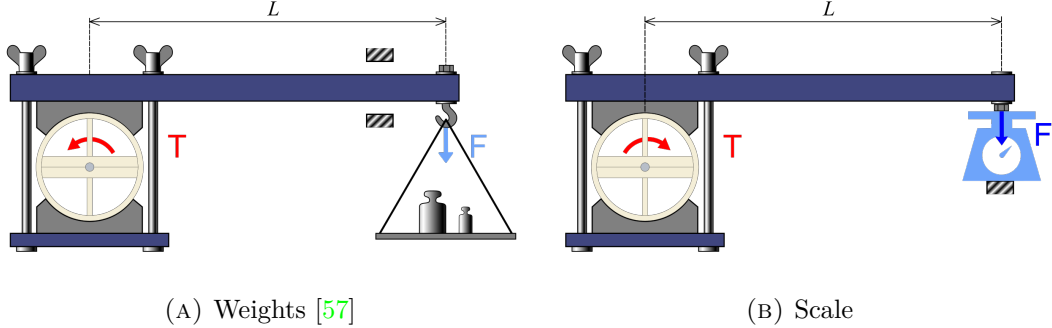


FIGURE 5.2: Theoretical method torque - Prony brake - basic implementations

In practice, it would be hard to balance out the torques perfectly to get the arm horizontal again. Instead, the arm is secured by a scale as shown on Figure 5.2b. Now the prony brake does not have to be balanced any more and a continuous measurement of the torque is possible. Equation 5.1 is still valid here. Note that this method is less accurate than using strain gauges, as some energy is lost in heat due to the friction between the clamp structure and the wheel.

Applied setup

The use of wooden blocks is not practical, so a belt can be used instead as shown on Figure 5.3. Instead of tightening the wooden blocks closer together, the belt can be wrapped around the wheel tighter by moving the top bar up. Torque causes a force on the belt in the direction of the rotation, meaning F_2 on the figure is larger. To obtain the force produced by only torque, two scales are needed to find T . Equation 5.1 still holds with L equal to the wooden wheel radius. The force F should be calculated by:

$$F = F_2 - F_1 \quad (5.2)$$

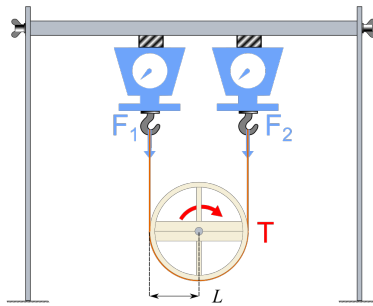


FIGURE 5.3: Theoretical method torque - Prony brake - belt and dual scales

Otherwise, the force as a result from tightening the belt and the force provided by the torque would be measured and the calculated torque would be incorrect. Only

5. TORQUE

one scale is needed if the clamp structure is made to rotate freely again. In addition to simplifying the setup, a more accurate result would be obtained because there would not be a combined uncertainty on the force readings. This can be achieved by hanging the clamp structure from a hinge, connected to a static gantry crane as seen on Figure 5.4. A single crane scale is hung to the right of the hinge. If the clamp structure is in balance when there is no torque applied, the crane scale detects no force. This balance is achieved by hanging a balancing weight on the opposite side of the chain hoist. The belt can be tightened by the chain hoist, without having any influence on the observed force. This is because both ends of the belt pull equally hard on the bar, transferring all the force to the hinge. The observed force is therefore the result of the torque provided by the water wheel only.

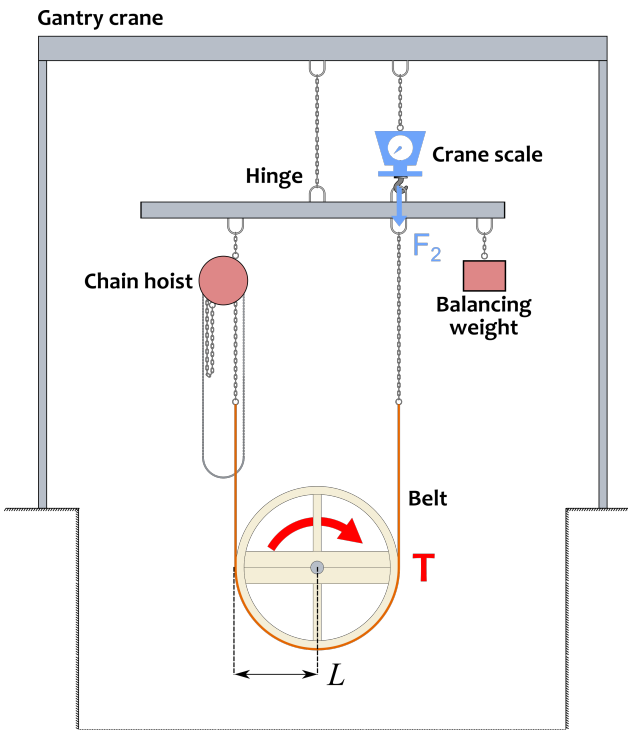


FIGURE 5.4: Theoretical method torque - Prony brake - hinged

5.1.3 Test bench

Test benches are used to characterise the torque/speed curves for motors by directly measuring the dynamic torque and the angular frequency. Based on this information and the electrical power provided, the efficiency η can be determined too. They work by coupling a test motor to another motor that can act as a variable load. Different sensors are in place to measure the parameters such as a tachometer and the previously discussed torque transducers. These sensors are connected to the control system, which processes the data and displays the results [52]. An example of a test bench is shown on Figure 5.5.

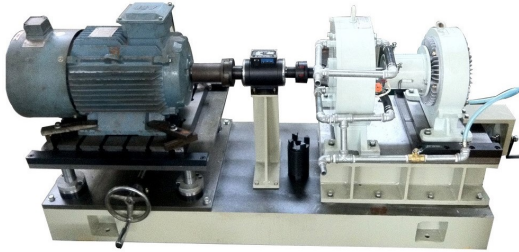


FIGURE 5.5: Theoretical method torque - motor test bench [58]

This method is by far the easiest and most accurate if used under the right circumstances. Most test benches (including the ones owned by the KUL) are rated for a high ν starting from 1000 r/min, making it difficult to use them for the studied site. As discussed in Section 3.4, the peak ν reaches only about 4 r/min. It is theoretically possible to increase ν by a gearbox, but the gear ratio would have to be enormous making it hard to produce. Instead, placing a smaller rubber wheel on the wooden wheel was considered to increase the rotational speed without using gears. This was deemed impossible because the radius would have to be minuscule. The calculation for this can be found in Appendix D.

5.2 Practical implementation: hinged Prony brake

The previous section discussed different methods to determine T , but only one seems suited. A custom force transducer is expensive and inaccurate if not used correctly and the test bench cannot work with such low ν . The hinged Prony brake is therefore selected as shown on Figure 5.4. The real life implementation is shown on Figure 5.6. Tests are only performed on mill 2, because there is no space to place the gantry crane over mill 1. The water wheels are built identically, so their torque/speed curve is assumed to be the same anyway.

As soon as measurements started, multiple issues came up that were solved in turn by creating multiple implementations.

5.2.1 Iteration 1: handheld tachometer

The first implementation uses a handheld tachometer so the instantaneous ν can be linked to the measured torque. If the custom tachometer is used where only one measurement is taken every rotation, it would take significantly longer to do all the tests. This method soon turned out to be inaccurate, because ν is too low for this type of tachometer as discussed in 3.1. As a result, the torque/speed points shown on Figure 5.7 didn't show any trend, which makes any form of power optimisation difficult. The power curve is found by multiplying the torque/speed curve by ν and generally has a clear, unique peak at ν_{max} . Finding this unique peak is impossible for this data.

5. TORQUE

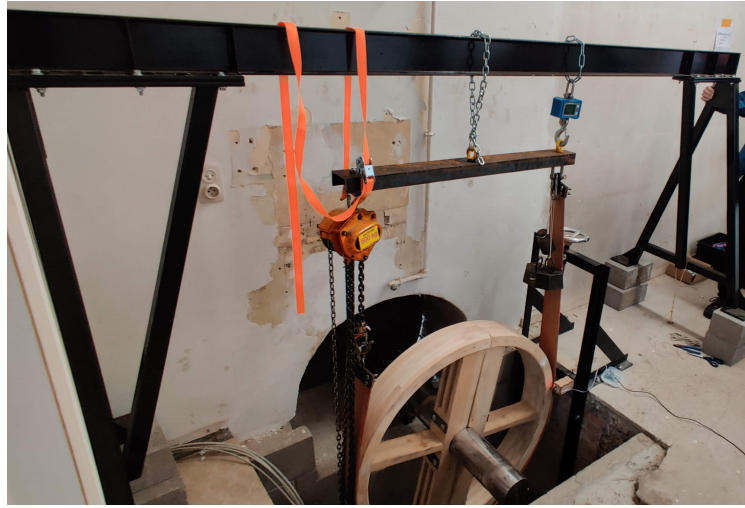


FIGURE 5.6: Practical method torque - hinged Prony brake

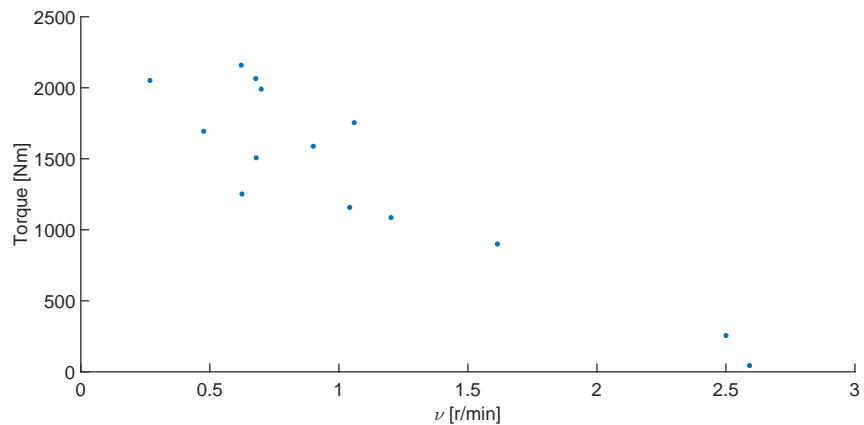


FIGURE 5.7: Rotational speed - handheld tachometer

5.2.2 Iteration 2: custom tachometer - multiple triggers

Original

Another implementation uses the custom Arduino tachometer. It can be adapted to include multiple trigger points to eliminate the accuracy problem and prevent having to wait for an entire rotation. This setup was already discussed in Section 3.5 and put forward another issue: inconsistent rotation. The established reason is rotational imbalance, which is not solvable without significant adaptations to the water wheels. This makes it impossible to use this implementation in the current state. All the ν data discussed in Chapter 3 was measured by a single trigger point and linking those points with the intermediate ν measured here would be impossible.

Spring adapted

Before the rotational inconsistency was properly investigated, the first hypothesis was produced under the condition that it had to be related to the Prony brake tests. The idea was that if the wooden wheel is not perfectly round, the belt would be tighter at positions where the radius is larger. This leads to more friction, a higher torque and thus lower speed. This hypothesis was partly correct, but not the main cause. The radius range of the wooden wheel is $0.545\text{ m} - 0.562\text{ m}$. The problem is mitigated by adding a spring to the setup, allowing for some margin in the belt's movement. The spring, shown on Figure 5.8, has a high spring constant so the given margin is small.

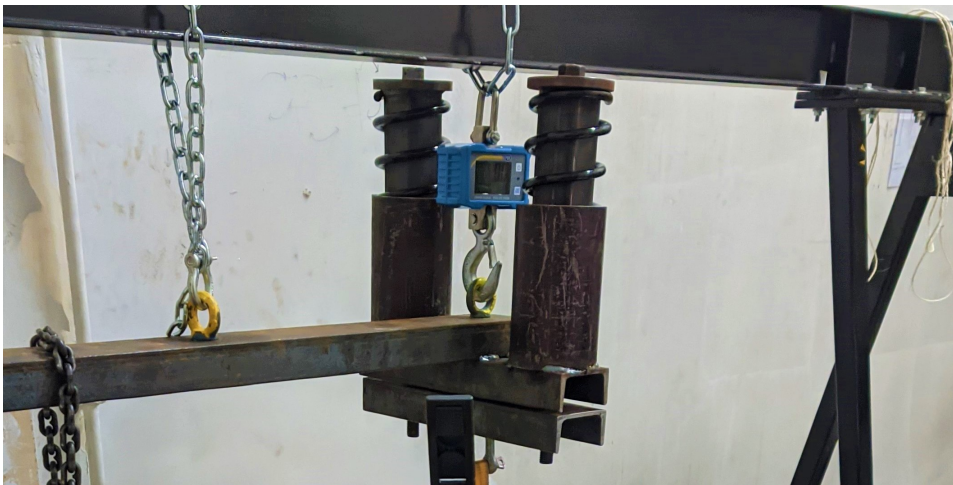


FIGURE 5.8: Practical method torque - hinged Prony brake - spring

5.2.3 Iteration 3: custom tachometer - single trigger

The third and final iteration uses the custom tachometer with a single trigger point so the ν data can be used as is. The rotational inconsistency causes the force to vary significantly over one rotation too. A solution is to measure the force continuously over a single rotation and then taking the average as the final result. This yields the average force and ν over one rotation, which allows for the calculation of the average power. The average force is multiplied by the minimum radius of the wooden wheel to get the conservative average T . The resulting error is only 3%, as torque is linearly dependent on the radius (which varies by 3% itself) according to Equation 5.1.

This iteration has a functional issue: the crane scale has no logging functionality. To overcome this limitation, a video of the crane scale screen was taken and Optical Character Recognition (OCR) was used to extract the force measurements from the video frames. This allowed for the continuous collection of force data. Custom OCR is developed in the next section to achieve the highest recognition and accuracy rate possible.

5.3 OCR

OCR is a type of software that can ‘translate’ text in images to machine-encoded text. In other words, it recognises characters and converts them into a useable format [59]. The images that need to be converted here are frames from a video of a seven-segment display showing force measurements from a crane scale. These types of displays are widely used and work by turning seven individual segments on or off to portray a single digit. Placing multiple seven segmented digits together forms a full number. There are OCR software packages in e.g. Google Tesseract or MATLAB that work out of the box. These packages were tested first, but recognition success and accuracy was low. Therefore, custom OCR software was developed in MATLAB specifically for seven-segment displays. Before the OCR can be used, the frames have to be preprocessed first to extract the useful information only and improve its quality. The entire flow of frame preprocessing and seven segment OCR is shown in Figure 5.9.

5.3.1 Frame preprocessing

A digital image consists of many pixels arranged in a grid that each have an individual colour. This colour is typically determined by an RGB triplet with intensity values ranging between 0 and 255, 0 being the lowest intensity and 255 being the highest [60]. The screen of the crane scale uses a screen with light blue backlight and dark blue segments as shown in Figure 5.12a. Image processing of every frame exploits this fact to isolate the digits and improve their quality.

First, the frame is cropped to the screen size and rotated to straighten the digits. Then the blue channel of the RGB triplets is isolated to create a greyscale image with the corresponding histogram as shown on Figure 5.10. The histogram quantifies how many pixels the image contains for every intensity. The higher the intensity, the lighter the shade of the pixel. A clear peak is present at the tail because most pixels in the image depict the light coloured backlight. The segments are depicted by darker pixels, so there is a clear distinction between the intensity range of the background and the segments. A cutoff intensity is selected by trial and error to remove the unwanted background pixels. All the pixels with an intensity above that cut-off are set to zero, with the new image and histogram shown on Figure 5.11 as a result.

More steps are required to get better image quality, but the visuals are excluded from this discussion to keep it more concise. They can however be found in Appendix E.1.1. The next step is to binarise the image effectively turning the greyscale into a black and white image. The possible intensities are now 0 or 1, 0 being a black pixel and 1 a white pixel. The remaining image still contains some pixels that do not belong to a digit and should be removed to prevent false detections. The image is split up in different areas consisting of white pixel clusters. The overall average number of white pixels in an area is calculated, which in turn can be used as a threshold value. All the areas containing less white pixels than half of this threshold are removed.

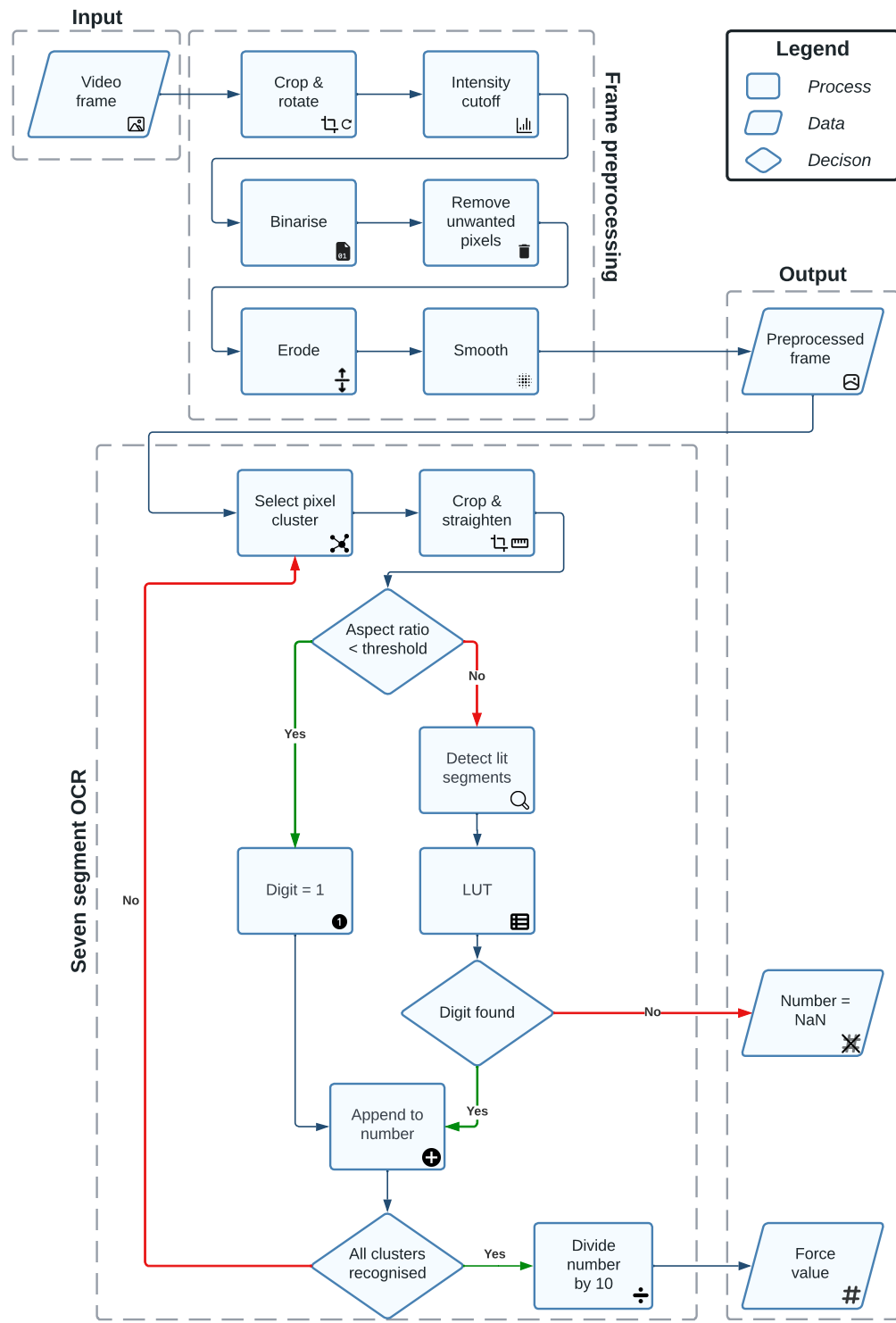
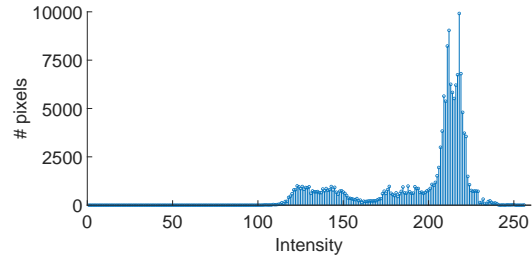


FIGURE 5.9: Preprocessing & OCR flowchart - crane scale seven segment display

5. TORQUE



(A) Greyscale image

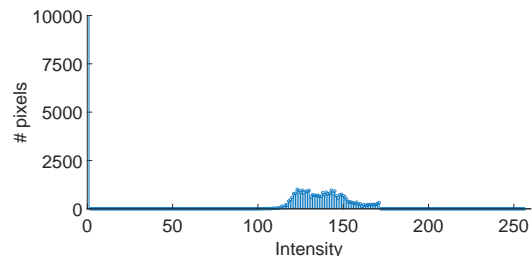


(B) Histogram

FIGURE 5.10: Crane scale frame - original isolated blue channel



(A) Greyscale image



(B) Histogram

FIGURE 5.11: Crane scale frame - cutoff isolated blue channel

This removes the comma from the image as well, which is solved in post by dividing the OCR result by 10. The only remaining areas are segments that are turned on. The next step is to erode the boundaries between the segments of a single digit. This lumps the separate areas of a single digit together into one big cluster of white pixels. Finally, the edges are smoothed out. The final result is shown on Figure 5.12b. This image is given as an input to the custom seven segment OCR, which is discussed in the next section.



(A) Original



(B) Preprocessed

FIGURE 5.12: Crane scale frame - original vs preprocessed

5.3.2 Seven segment OCR

Now that the frame is preprocessed and every pixel cluster represents a digit, a simple form of OCR can be developed specifically for seven segment displays. Its working principle is discussed first, before evaluating the accuracy and recognition rate.

Working principle

The underlying theory of a seven segment display can be exploited to accurately detect the digits. Every digit between 0-9 can be represented by turning seven segments on or off if they are arranged as shown in Figure 5.13a. Every digit can then be represented by a binary number with a fixed length of seven. A 1 corresponds to a segment that is on and a 0 a segment that is off. The example on Figure 5.13b shows a 6 that is formed by the lit segments A, C, D, E, F, G. Segment B is off and thus the resulting binary representation is 1011111.

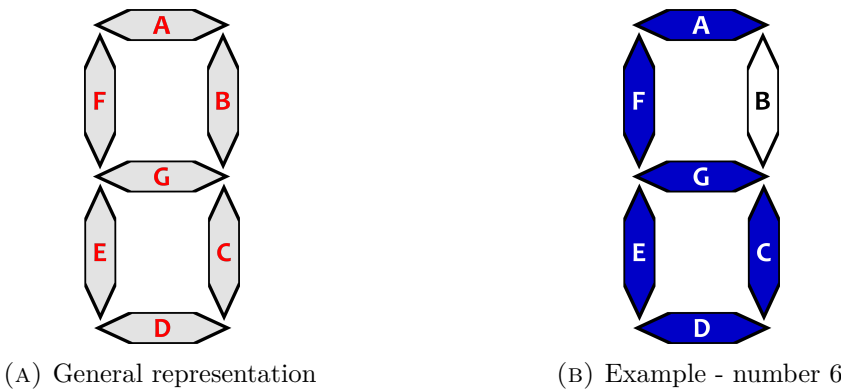


FIGURE 5.13: Seven segment display theory

The seven segment OCR algorithm exploits this in reverse order. A preprocessed frame is given as an input. First, the separate clusters are found. These are iterated over from left to right. Figure 5.14a outlines the clusters by a red box, each clearly containing just one digit. The cluster is cropped and straightened so the segments are always placed in the same location. There are now seven different locations on the image, each corresponding to a segment. These locations are checked one by one and labelled on (1) or off (0) as shown in Figure 5.14b. If there are more white pixels in the location, the segment is on or “lit”. If not, the segment is off or “not lit”. Combining these labels forms a binary number with a fixed length of seven again. This binary number is given as an input to a lookup table (LUT), effectively translating the pixel cluster into a digit. These steps are repeated for each cluster and appended to the previous digit(s). If all clusters have been recognised, the number is divided by 10 to compensate for the earlier comma deletion. The final result represents the force value displayed by the crane scale, which is 61.6 kg in the example. For reference, the OCR software provided by MATLAB returned 5.5 kg.

5. TORQUE

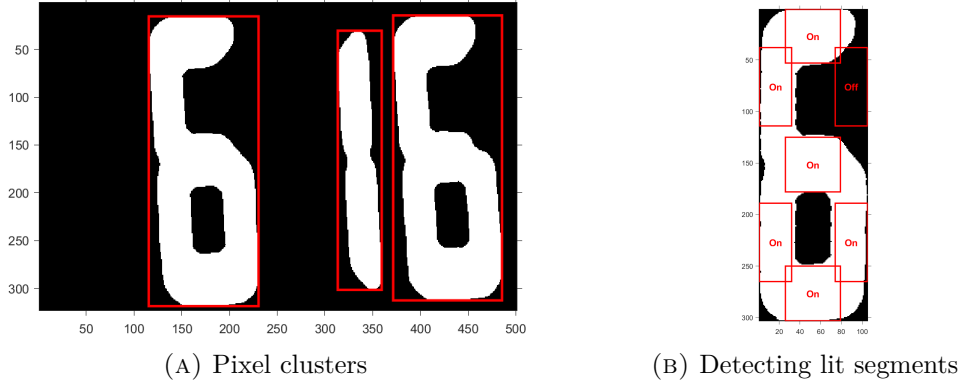


FIGURE 5.14: Seven segment OCR - frame detection

Note that using the segment locations to detect a 1 would be impossible. The cluster would be cropped to a narrow rectangle only containing white pixels. If the original locations would be used then, a 1 would always be recognised as an 8. This is because all the segments are labelled as lit as there are only white pixels present in the cluster. Therefore, the aspect ratio of the cropped and straightened cluster is always checked. If it is smaller than a threshold value (determined by trial and error as 0.34) it is narrow and therefore the digit has to be a 1.

Accuracy and recognition rate

Also note that analysing video frames of a seven segment display inherently has shortcomings. Some illegal binary sequences might arise as the segments fade away instead of disappearing immediately. These are not in the LUT and the output will therefore be a “NaN” value. Another possibility is that segments that are not directly connected still appear to be lit. This creates two separate white pixel clusters and results in a value that is one order of magnitude greater than neighbouring values. These values are removed in post by comparing every value to its neighbours and removing outliers. Examples of these occurrences are included in Appendix E.1.2.

Throughout testing, 83 % of the frames were recognised as a real value. Of the recognised frames, 98.94 % were deemed correct. The video was filmed at 30 frames per second and 1 frame in 10 is analysed. The recognition rate and accuracy is therefore deemed sufficient to calculate the average force over one rotation using the seven segment OCR algorithm.

5.4 Results

Now that the force can be logged over a full rotation, different measurements have to be taken to find the torque/speed curve. The chain hoist is used to tighten the belt to a certain setting. Different settings are used, so a range of average T is found between the no-load ν_{nl} and standstill. Note that the previously discussed

rotational speeds were always considered to be no-load speeds. Here, an explicit distinction is made between the no-load speed ν_{nl} and speeds under load ν_l . These tests have to be performed at different ν_{nl} to be able to accurately characterise the torque/speed curves over the full no load ν range found in Chapter 3. Figure 5.15 shows an example of the force evolution over a full rotation for $\nu_{nl} = 1.05$ r/min for a total of 9 settings. Setting 0 represents standstill and is shown in the top left corner. The belt is systematically tightened with setting 1 being the loosest setting and setting 8 being the tightest. Note that the crane scale displayed force in kg and this graph is in newton.

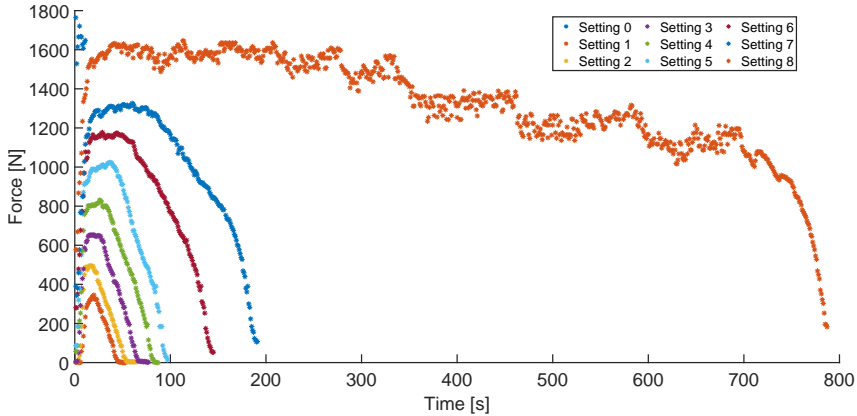


FIGURE 5.15: Arenberg water wheel - force evolution for one full rotation

The force evolution shows a clear maximum similar to the chronological inconsistent ν from Figure 3.7d. Here, it is most likely due to two factors: still the rotational imbalance, but also the radius variation that tightens the belt and produces higher forces at larger radii. As explained before, the latter effect is mitigated by the spring but cannot fully be removed.

The force measurements are repeated a total of three times for each setting to indicate the results are reproducible. Every repetition is averaged and multiplied by the minimum radius to form a single torque value. The rotational speed for every repetition is measured too and matched with the torque value. This results in the torque points shown on Figure 5.16.

A curve is fitted to these points, resulting in the following equations for the torque:

$$T_{0.85}(\nu_l) = 504 \nu_l^2 - 1024 \nu_l + 512 \quad (5.3a)$$

$$T_{1.05}(\nu_l) = 386 \nu_l^2 - 1232 \nu_l + 874 \quad (5.3b)$$

The subscript of the torque T refers to the ν_{nl} at which the tests where performed.

5. TORQUE

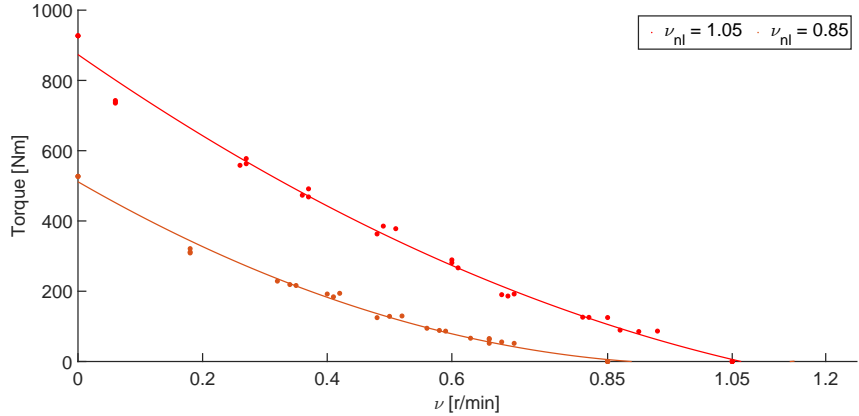


FIGURE 5.16: Arenberg water wheel - torque/speed curves

The fitted curves have an R^2 value of 0.998 and 0.997 respectively. The residuals are added in Appendix E.2 and show no discernible pattern. This indicates that the chosen quadratic regression is a good choice.

These tests take time and are obviously dependent on river parameters to attain different ν_{nl} . During the period when these test were performed, mill 2 was mostly at standstill due to low flow rates. Therefore, it was only possible to characterise torque/speed curves at two different ν_{nl} . These ν_{nl} are at the low-end and more measurements with higher ν_{nl} should be taken before results can be extrapolated.

5.5 Conclusion

This chapter discussed multiple methods to measure torque and selected the Prony brake method as the most suited one. The practical implementation encountered several issues, resulting in multiple iterations eventually settling at measuring the average torque over one full rotation. Custom seven segment OCR software was developed to account for the lack of logging capabilities in a regular crane scale. The recognition rate and accuracy of this software is high, making it a valid replacement for direct logging. The software is used to measure the average torque for two different no-load speeds at multiple load settings. Every load setting was measured three times to ensure the results were reproducible. The results at every setting were plotted and a curve was fitted to these points. These curves are the torque/speed characteristics and can be used in the next chapter to determine the produced power. More torque/speed curves should be characterised at higher ν_{nl} , which is impossible for the current river conditions and is therefore marked as future work.

The next chapter sets the framework for calculating the produced power P_{mech} for the characterised torque/speed curves. Should more torque/speed curves be characterised, the corresponding power curves should be evaluated too.

Chapter 6

Power

The previous chapter characterised the torque/speed curves for two different ν_{nl} . The power equation can directly be calculated from these curves by multiplying the torque and speed values at each point on the torque/speed curve. No accurate financial analysis can be performed for only two power curves, but an attempt is made. It is also possible to calculate the hydraulic power from the river parameters. These powers can be used to calculate the efficiency.

6.1 Water wheels

The mechanical power delivered by the water wheels can be calculated using Equations 1.1 and 1.2:

$$P_{mech,\nu_{nl}}(\nu_l) = T_{\nu_{nl}}(\nu_l) \cdot \nu_l \cdot \frac{2\pi}{60} \quad (6.1)$$

The specific power equations for the defined torque/speed curves can be calculated by plugging Equation 5.3 into 6.1:

$$P_{mech,0.85}(\nu_l) = (504 \nu_l^3 - 1024 \nu_l^2 + 512 \nu_l) \frac{2\pi}{60} \quad (6.2a)$$

$$P_{mech,1.05}(\nu_l) = (386 \nu_l^3 - 1232 \nu_l^2 + 874 \nu_l) \frac{2\pi}{60} \quad (6.2b)$$

The mechanical output power can be maximised using these equations and maximum power point tracking (MPPT).

6.1.1 MPPT

Maximum power point tracking is a technique used to optimize the power output of a system, widely used for solar panels. The goal of MPPT is to operate the system at the point on its power curve where it is producing the maximum amount of power. In solar panels, an MPPT converter monitors the voltage and current output and adjusts these to get the MPP. The same idea can be used to determine the MPP or P_{max} of the water wheels. $P_{mech,\nu_{nl}}$ is a function of the load rotational speed ν_l ,

6. POWER

which can be measured and adjusted as well. Just as in MPPT for solar panels, multiple approaches can be taken to find the MPP while the system is in operation. The details on this are outside the scope of this thesis.

The ν_{max} is the point at which the power is at its maximum. The power curves $P_{mech,0.85}$ and $P_{mech,1.05}$ and their respective MPP are shown together with their speed/torque curves on Figure 6.1. The relevant data is presented in Table 6.1 as well.

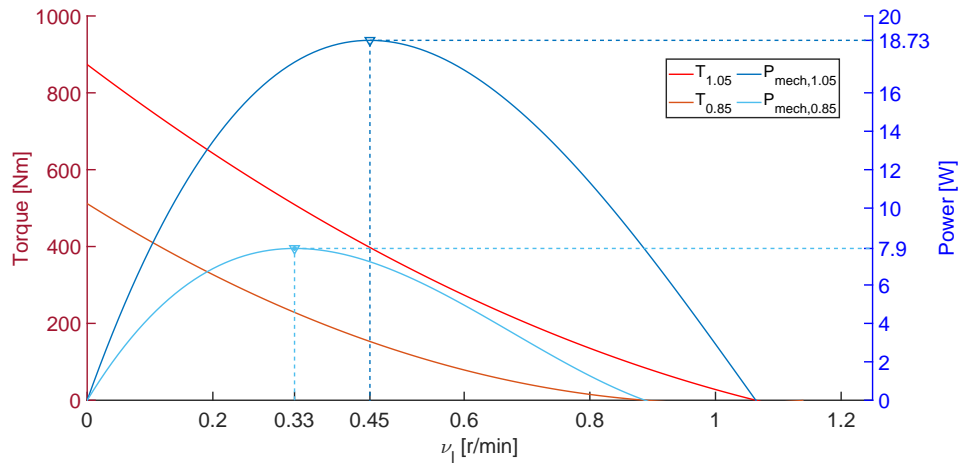


FIGURE 6.1: Arenberg water wheel - power curves

6.1.2 Extrapolation

Similar to a power curve of a wind turbine, a power curve for the water wheel can be characterised. For wind power curves, the output power is a function of the wind speed. For the water wheel power curve, the output power is a function of the no-load speed. Using the model from Chapter 4, it can eventually be turned into a function of water level. This enables the ability to implement an MPPT algorithm using external data. Because the river parameters are forecasted, it would allow for energy forecasting as well. As mentioned before, more measurements should be taken to accurately extrapolate the power for higher ν_{nl} . However, an attempt at extrapolation can still be performed to get an idea of the order of magnitude the mills can produce. If the maximum power points are assumed to be related through a power curve ($a x^b$), an equation can be formulated that puts P_{max} in function of ν_{nl} using the points of Table 6.1:

$$P_{max}(\nu_{nl}) = 15.345 \nu_{nl}^{4.0853} \quad (6.3)$$

As seen in Section 3.4, the average ν_{nl} is 2.24 r/min for mill 1 and 2.13 r/min for mill 2. Using these results in Equation 6.3, the corresponding powers would be 413.8 W and 336.9 W respectively or about 750 W in total.

6.1.3 Economic feasibility

Because the extrapolation is most likely in the same order of magnitude as the actual powers would be, it is clear that the watermill will most likely never be able to produce electricity in an economically feasible manner. The maintenance costs and investment costs of a generator, possible power electronics, a gearbox, protection devices, control systems, etc. can most likely never be earned back by the costs saved on the electricity bill. A back-of-the-envelope calculation can be made to support this statement. The KU Leuven buys its electricity at a price of 170 €/MWh (or 0.00017 €/Wh). Assuming the mills deliver a joint constant power of about 750 W, this would be the equivalent of € 0.1275 saved every hour or about € 1,116.9 on a yearly basis. If a relatively significant payback period of 20 years is allowed, the maximum investment and maintenance costs are equal to € 22,338. Considering the amount of needed hardware, the necessary investment costs alone are most likely higher.

Note that the energy market is distorted due to high gas prices at the time of writing this thesis and that the KUL used to buy its electricity at 100 €/MWh. Both prices include federal tax. Also note that these calculations do not take into account factors that can have a significant impact on the actual cost saving. On the financial side inflation and tax requirements should be considered. On the electrical side the capacity factor is assumed to be 1, the generator and power electronics are assumed to have 100% efficiency and the mills are assumed to have a similar rotational speed profile every year. The first two electrical assumptions are more than likely a significant overestimation of reality. The last assumption is even more problematic, as indicated by the significant change in flow rate that was portrayed by the Q(h) curves in Section 4.2.2 resulting in a much lower ν for the same h .

6.2 Hydraulic

The hydraulic power is calculated at the same ν_{nl} as the torque/speed curves are analysed for, using Equation 1.3 and 1.4:

$$P_{in} = \rho \cdot g \cdot v \cdot A \cdot H \quad (6.4)$$

The measured parameters are shown in Table 6.1, as well as the resulting power. Note that there is only a slight change in head and thus most of the increase in power is due to the higher flow rate. This is in line with the data presented in Chapter 4, where it was shown that the head across the site is kept relatively constant and the main influence is due to the flow rate.

Note that the value for H and A is always the same, because the blades are 1 m wide and have a rectangular shape. The surface where the water flows against is therefore equal to:

$$A = H \cdot 1 \text{ m} = H \text{ m}^2 \quad (6.5)$$

6. POWER

6.3 Efficiency

Finally, the efficiency can be calculated using Equation 1.5. These efficiencies are very low as expected, most likely mainly due to the nature of the placement as described in Section 2.2.1. Should the improvements proposed in that section be made, the efficiency could reach up to 85% causing drastic increase in power generation. Note that the calculated efficiencies are close to the worst case efficiency of the radial subtype discussed in Section 1.1.1 as expected due to the fact that the water wheels can be considered of the radial subtype for the current setup. Also note that only two values are calculated, which is not enough data to make final conclusions on the efficiency of the system. The efficiency is not a fixed number, but varies significantly with river parameters also as expected.

TABLE 6.1: No-load rotational speeds ν_{nl} with corresponding rotational speed set points, maximum power points, hydraulic powers and efficiencies

ν_{nl} [r/min]	ν_{max} [r/min]	P_{max} [W]	v [m/s]	A [m^2]	H [m]	P_{in} [W]	η [%]
0.85	0.33	7.90	0.66	0.11	0.11	78.34	10.08
1.05	0.45	18.73	0.74	0.14	0.14	142.28	13.16

6.4 Conclusion

The power curves for the two available no-load speeds were calculated in this chapter based on the torque/speed curves. The resulting maximum powers are low, making it unlikely for the Arenberg site to generate electricity in an economically feasible manner without changes made at the site. The efficiencies of the water wheels were determined at the same no-load speeds using calculated hydraulic powers. These efficiencies are low and comparable to the radial subtype efficiency, as expected. Should the proposed improvements from Section 2.2.1 at the site be made, the efficiency could reach up to 85% causing drastic increase in power generation. This would make electricity generation at the site much more probable.

This research is now at a crossroads with two possible exits. First, it is possible to do more specific research on the needed hardware to make a fully working pico hydro plant. An optimisation algorithm can be written that takes maintenance costs and all the other factors that were omitted in the back-of-the-envelope calculation, different hardware options, etc. as an input and outputs multiple possible roads to take. Even if this algorithm outputs a reasonable option, the low capacity does not have a significant impact on the energy mix profile of the university.

Second, the next actions are in line with the original idea of restoration: aesthetics. A website can be developed to show the real-time ν_{nl} information, the history of the watermills and the research performed in this thesis in an accessible manner. The website can be used a basis for educational purposes or create general interest in the

--- 6.4. Conclusion

landmark as a whole.

The second exit is considered to have the most impact for the data currently available and therefore the website was set up. It is shortly discussed in the next chapter as some operational functionality is present that might be useful should the power plant ever be built.

Chapter 7

Website

Although it is unlikely the Arenberg watermill will ever produce power with the current site, it is still of great importance to KUL alumni, staff and students alike. To make sure it receives the recognition it deserves, a website is developed that describes the history, the current state and the potential future through additional research. At the time of writing this thesis, the website is available at: “<https://arenberg-watermill.github.io/>”.

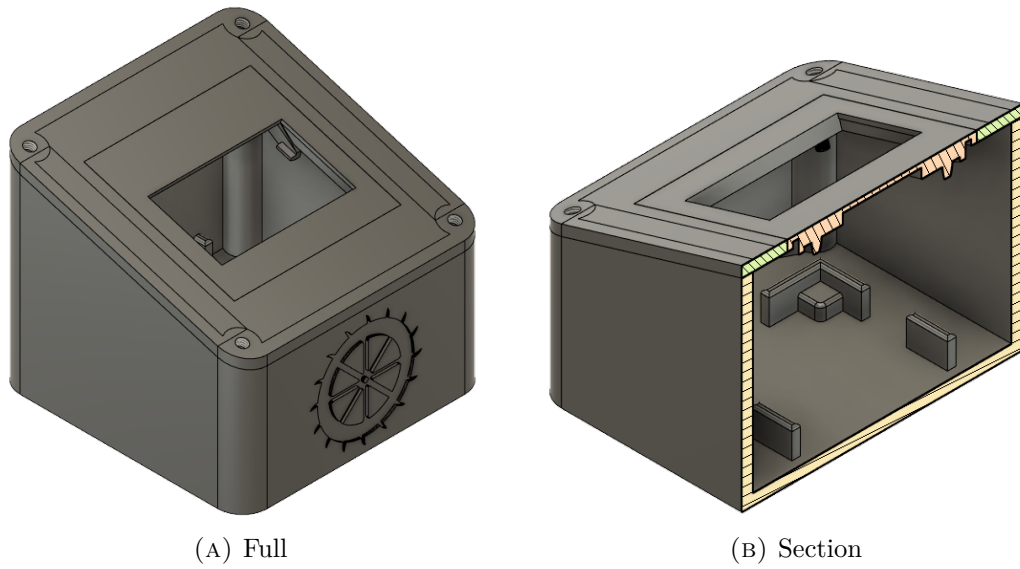
This chapter briefly discusses an improved version of the tachometer discussed in Chapter 3, the framework used to facilitate the website and the operational functionality. These concepts are only discussed briefly as the exact mechanisms are considered irrelevant to this thesis. The actual website contents can be found on the website itself. A screenshot of the home page is included in Appendix F. Note that not all research is added at the time of submitting this thesis and more content will be added soon.

7.1 Custom tachometer v2

As mentioned in Section 3.2, a campus wide WiFi network was made available in the summer of 2022 specifically for IoT devices. This allows for a microcontroller with a WiFi chip to connect to the internet and therefore makes it possible to inspect ν remotely and in real-time. The need for an SD card and an RTC module disappears and the Arduino microcontroller was replaced by a much cheaper ESP8266-based chip: the Wemos D1 mini. The updated tachometer schematic is available in Appendix B.

The working principle remains the same as version 1, but instead of saving the measured rotational speed to an SD card it is directly uploaded to the internet. The data is sent to a Google Sheet through a web app.

7.1. Custom tachometer v2



(A) Full

(B) Section

FIGURE 7.1: Custom tachometer - v2 - 3D model

A custom case for the hardware was designed in Fusion 360 as shown on Figure 7.1. This case was 3D printed and installed as shown on Figure 7.2. The rotational speed is still shown locally, but is also available to the public through the website.



(A) Sending data

(B) Visual feedback ν

FIGURE 7.2: Custom tachometer - v2 - installation

7.2 Framework

The website was developed using Jekyll and is hosted through GitHub Pages. This setup does not allow for real-time data integration out of the box, so Google Sheets and Apps Script are used as an intermediary to facilitate the data processing. A web app is created through Apps Script so the tachometer can send over data through a simple GET request to a public URL. These services are all free to use and highly flexible.

The data is sent over an insecure connection and to a public URL. This means that, in theory, anyone could access the public URL and post their own data to the web app. Since this is no issue for the current use where the data is just displayed publicly, these security concerns are not addressed. Should the site ever be in use for electricity generation and the data used for control purposes, these concerns should be tackled. Note that the “public” URL does not mean anyone with an internet connection can just post data as the script deployment ID is needed. This is a 72 character string containing letters, digits and special characters that is not public, which makes unauthorised access improbable.

7.3 Operational functionality

The described framework allows for online data processing, removing the need for some steps found in the flowchart of Appendix C.2. For example, the quarter-hour intervals are created instantly and can be used to make a more accurate model of $\nu(Q)$ as described in Chapter 4 should this ever become possible.

Some extra functionality is available too. First, the power formula from Equation 6.3 is used to display an estimate of the potential mechanical power produced. Again, this power is the result of a poor extrapolation and should be updated with new torque/speed curve measurements. This functionality is just a proof of concept for now. Second, a graph of ν is created and updated using the interval data and displayed on the website as well. Screenshots of the real-time page are included in Appendix F. Finally, if one of the water wheels has not been turning for a certain time, an email is automatically sent to the technical services so they can assess the situation. Often, clearing the debris from the trash rack is enough to remedy the issue.

7.4 Conclusion

A website was developed using various free platforms to display the research performed on the watermill, the site history and the real-time rotational speed and potential power production. The rotational speed is measured by an improved version of the custom tachometer and published through a web app. Note that the historical data should be checked and elaborated on in cooperation with the KU Leuven.

Chapter 8

Conclusion

In this thesis, research was performed on the Arenberg water wheels to assess their (economic) feasibility of electricity generation. While no definite answer on this feasibility can be produced due to extreme droughts leading to a lack of measurement opportunities, a framework has been worked out to facilitate further investigation.

A site description was given and reasons why it cannot be adapted in a way that changes the environment were underlined. However, possible improvements in terms of efficiency were proposed and can be implemented without having any impact on the surroundings. These include reversing the orientation the wheels, placing a weir at their inlets and solving their rotational inconsistency. This inconsistency was investigated and attributed to rotational imbalance of the wheels most likely caused by poor built quality. A site visit to a VMM control station provided interesting insights into the inner workings of the control of river parameters and how they are measured.

A custom tachometer was designed and built to continuously and accurately measure the mean rotational speed ν at every rotation. These measurements are published on a dedicated public website that contains additional information on the site as well. Further processing of this data allowed for a model that characterises ν in function of the water level h measured by a VMM station upstream. The model provides reasonable accuracy under certain $Q(h)$ river conditions. Inaccuracies are largely attributed to the unpredictability of debris build-up in the trash rack. To improve the accuracy, regular maintenance, a more coarse trash rack, or an automatic trash rack cleaner were proposed. This model can be used to retrospectively estimate or forecast ν using historic or forecasted h data.

In the pursuit of characterising the torque/speed curves of the watermills, dynamic torque measurements were taken by an adapted Prony brake. This measurement suffered from multiple complications, which were solved by iterating on improved implementations. The final iteration makes use of custom developed OCR software and measures the average torque over a rotation. Only two different torque/speed

8. CONCLUSION

curves were characterised due to insufficient variation in no-load speeds caused by extreme droughts. The results were found to be reproducible and reliable, providing a solid basis for further analyses.

The power curves for the aforementioned no-load speeds were calculated using the torque/speed curves and the maximum power and their corresponding load speeds were found. The measured maximum powers are only in the 10 W range, but seem to be highly sensitive to changes in ν . The corresponding efficiencies at these maximum powers are only around 10%, which is in line with a radial water wheel design. Should the aforementioned improvements be made, the efficiency could reach up to 85% causing drastic increase in power generation and making electricity generation feasibility much more likely.

8.1 Future work

The characterised model suffers from a few caveats causing model invalidity at certain conditions. To improve the validity, more measurements for both mills should be taken at varying $Q(h)$ river conditions or ideally a direct flow rate measurement should be taken at the inlet of the mills so a single model that is always valid can be produced.

More torque/speed curves should be characterised to be able to accurately extrapolate the power generated at a certain no-load speed. This data can then be used to build an optimisation model that takes into account multiple hardware options, river conditions, different types of costs to provide an accurate financial analysis on the electricity generation feasibility.

In summary, the study has provided valuable information on the potential of the Arenberg watermill as a source of renewable energy. While the site has limitations, such as the effects of the water level on the ecosystem, the proposed solutions and recommended improvements show promise for increasing the efficiency and effectiveness of potential electricity generation at this site. With further research and implementation of these recommendations, it is not ruled out that the Arenberg watermill will once become a valuable source of renewable energy for the KUL.

Appendices

Appendix A

VMM stations

A.1 Station K08_012 - water levels

Figure A.1 shows a graph provided by the VMM to indicate at which water level threshold the flooding area starts to fill up. Figure A.2 shows at which water levels the area is filled up for 25%, 50%, 75% and 100%. It clearly shows the flooding of July 2021.

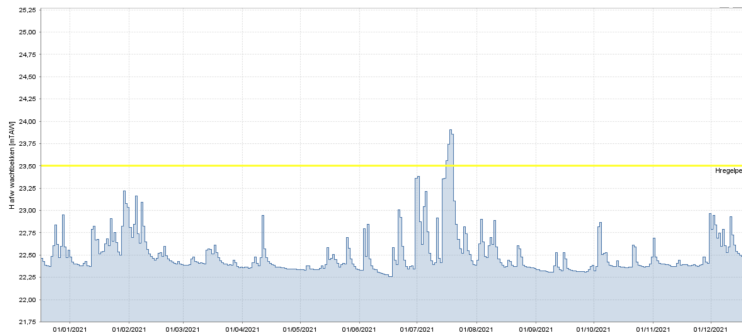


FIGURE A.1: Station K08_012 - downstream water levels and threshold of 23.5 mTAW

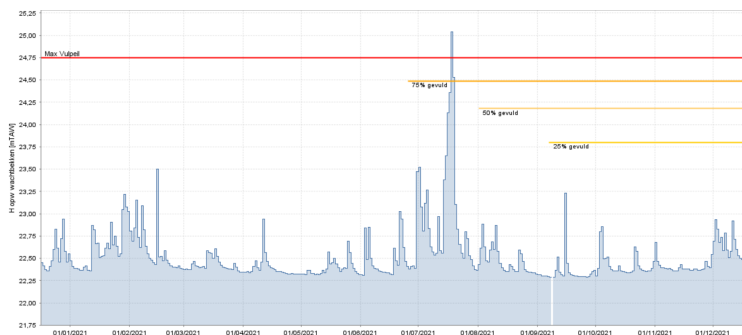


FIGURE A.2: Station K08_012 - upstream water levels and filling stages of flood area

A.2 Maps

Figure A.3 shows the location of all the discussed VMM stations, this time including the station at Sint-Joris-Weert used for flow rate data.

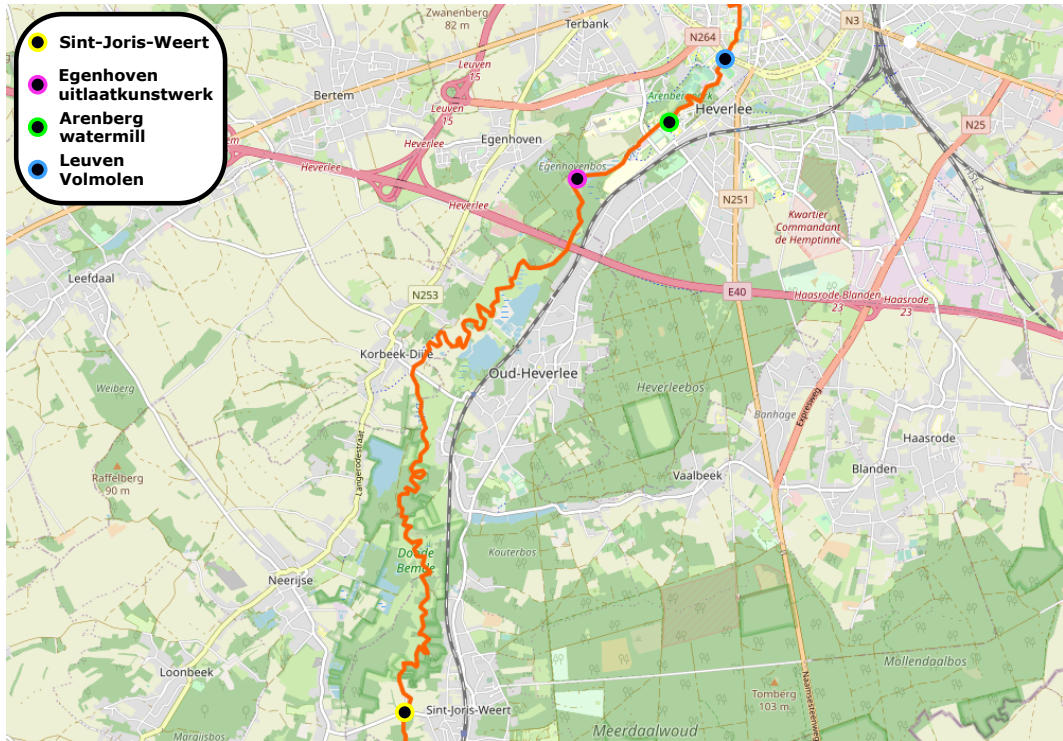


FIGURE A.3: Arenberg site - location of the closest VMM stations - including SJW

Appendix B

Custom tachometer

This appendix includes the circuit diagrams for both versions of the custom tachometer on Figure B.1 and B.2.

B.1 Version 1

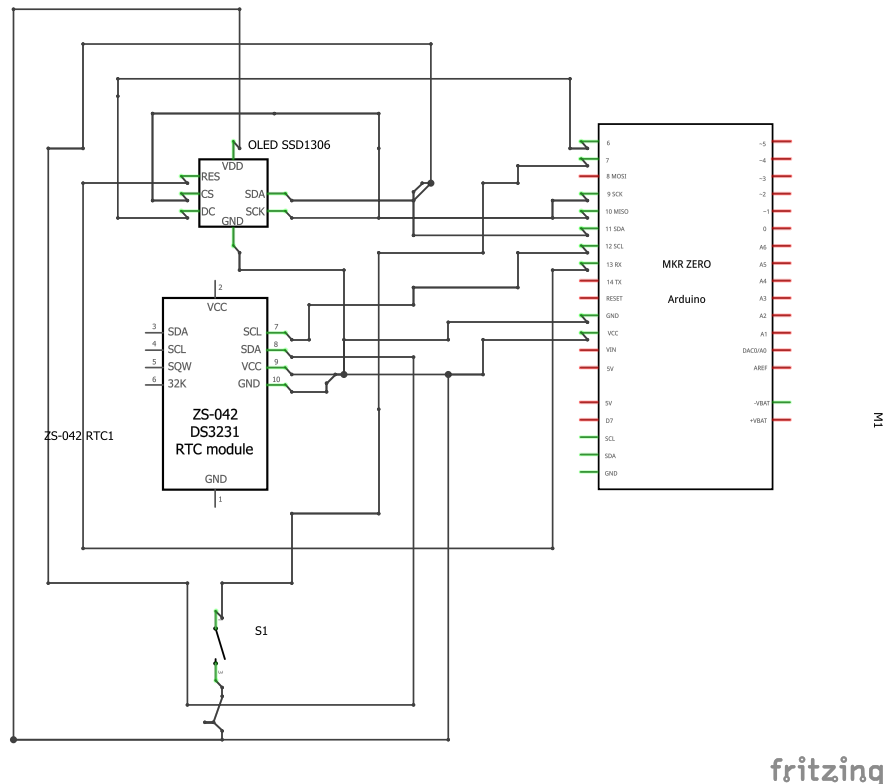


FIGURE B.1: Custom tachometer - v1 - circuit diagram

B.2 Version 2

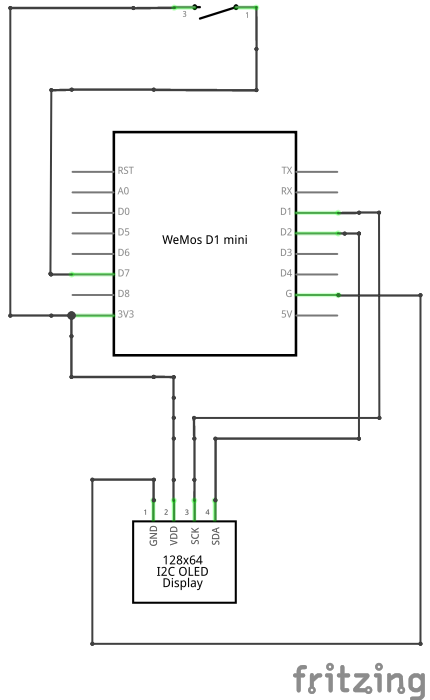


FIGURE B.2: Custom tachometer - v2 - circuit diagram

Note that the OLED module uses I2C instead of SPI as a communication method with the microcontroller, causing a simpler connection with only 4 wires instead of 7. An extra photo of the internal wiring of v2 is shown on Figure B.3.



FIGURE B.3: Custom tachometer - v2 - internal wiring

Appendix C

Modelling

C.1 Quality levels VMM

This section shows the codes used by the VMM to indicate the quality of a measurement. Only the codes marked 'excellent' and 'good' are used in this research.

TABLE C.1: Quality codes - VMM data

Data quality	Code 1	Code 2	Code 3
Excellent	10	110	/
Good	30	100	130
Moderate	50	150	/
Poor	70	170	/
Estimated	80	180	/
Suspect	90	190	/
Default	220	/	/
Missing	-1	/	/

C.2 Flowchart

The complete flowchart used through Chapters 3 and 4 to keep track of all the operations performed on the rotational speed and river data in the pursuit of forming a model between them is shown on Figure C.1.

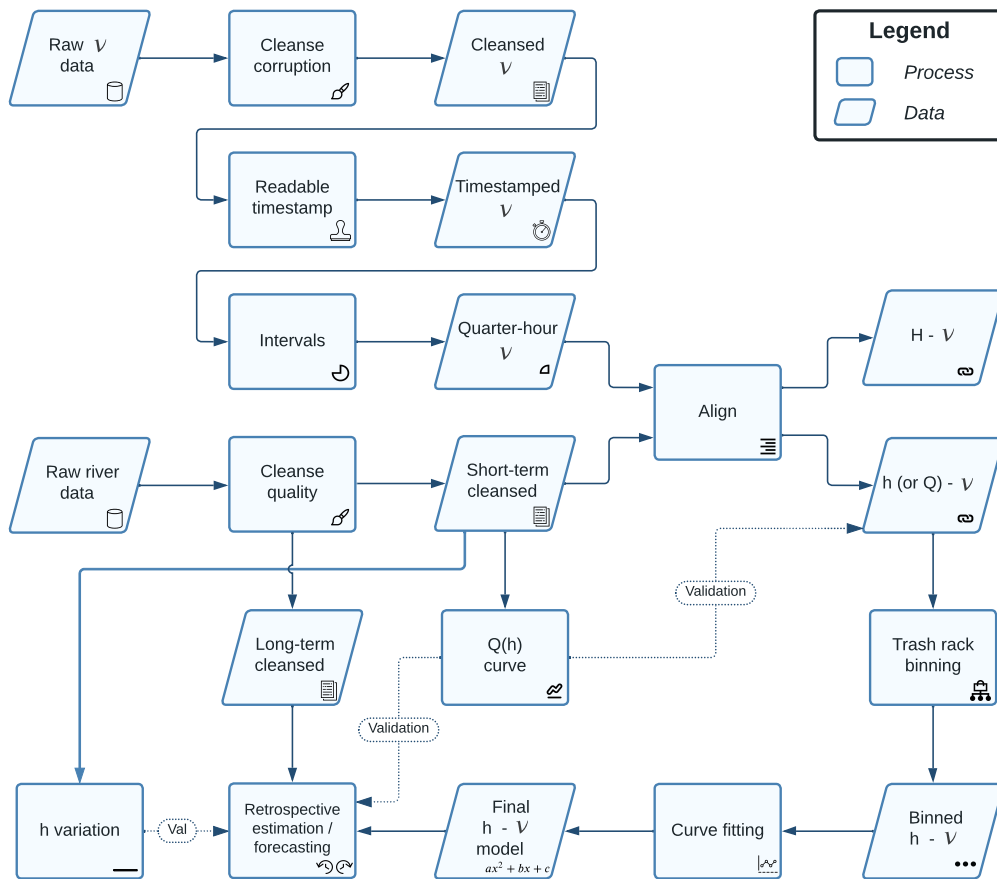


FIGURE C.1: Modelling flowchart - all operations on the rotational speed and river data

C. MODELLING

C.3 Extra plots

This section contains extra plots for the modelling that were not considered vital to the understanding of the modelling chapter.

Figure C.2 shows the scatter plot of ν in terms of water levels from the Volmolen station downstream from the mills. The relationship between both data resources is much less clear and therefore the Egenhoven station was selected.

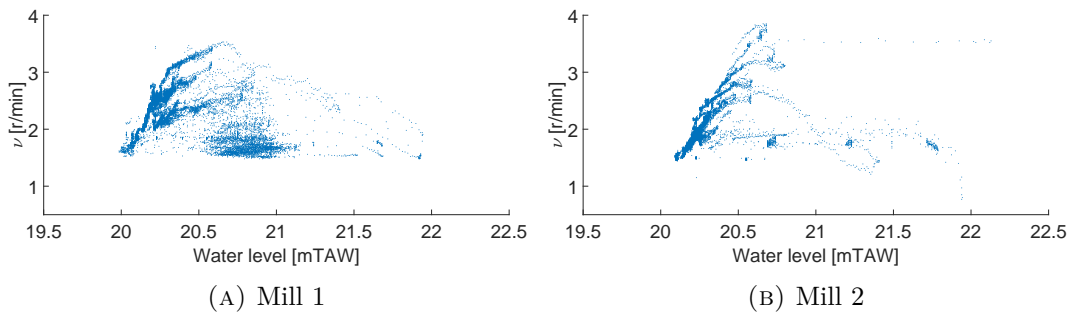


FIGURE C.2: Rotational speed - function of water level - Volmolen

The final models were fitted by a quadratic curve and the R^2 values were discussed. The residuals are shown on Figure C.3 and show no discernible pattern, reaffirming the choice for a quadratic fit. Note that the residuals for mill 2 are significantly smaller as the fit is better.

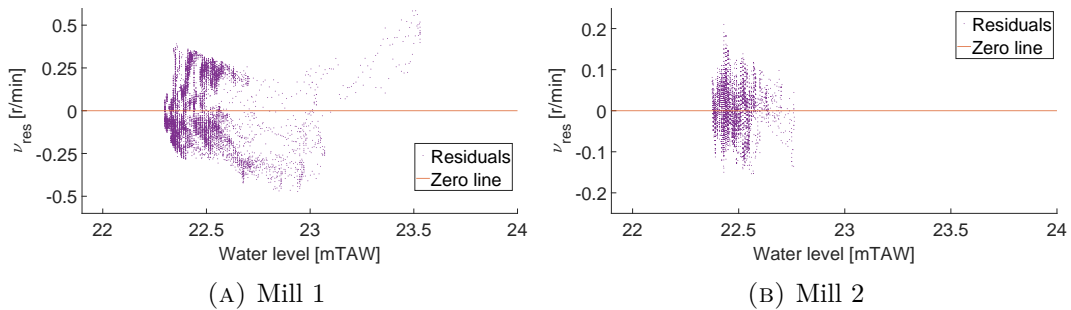


FIGURE C.3: Rotational speed - function of water level - final model - residuals

The model is valid half of the time which implies some kind of reoccurring effect in the $Q(h)$ data points. The points were marked winter (Jan-Jun) and summer (Jul-Dec) to test this hypothesis, but no discernible pattern is found on Figure C.4. A plot was even made that marked the points by month separately to get full certainty about the non-presence of the effect, but is excluded as again no pattern was found.

C.3. Extra plots

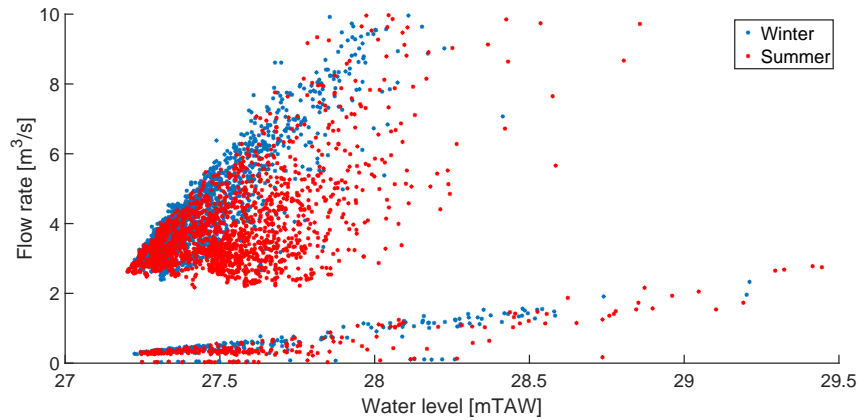


FIGURE C.4: Q(h) data points divided in winter and summer - SJW

The model can be used for forecasting using the forecasted water levels provided by the VMM. An example of this forecasting is shown on Figure C.5.

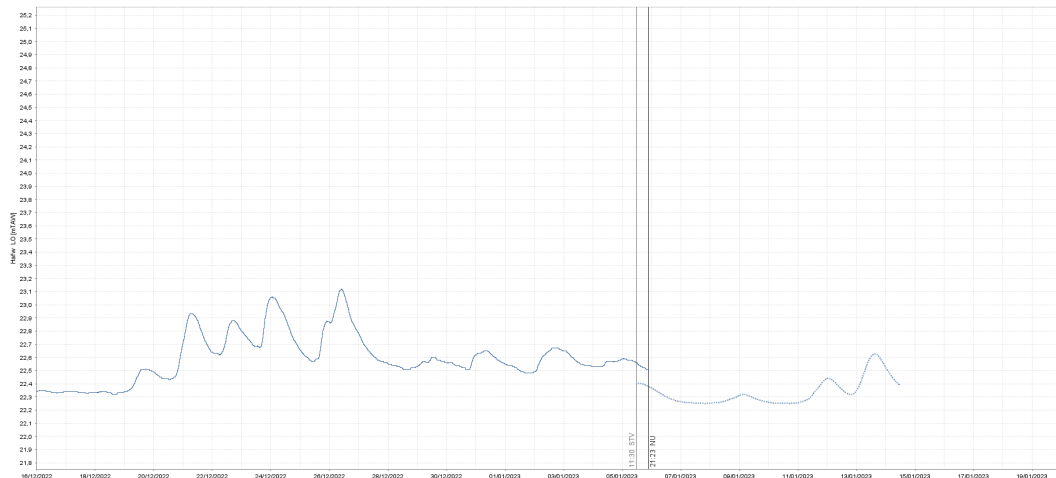


FIGURE C.5: Station K08_012 - forecasted water levels - Egenhoven

Appendix D

Rubber wheel sizing

This appendix shows the calculations performed on the feasibility of placing a rubber wheel against the inside wooden wheel to increase the rotational speed to 1000 r/min so a test bench can be used for torque/speed measurements. The radius of such a wheel would have to be 1.425 mm, which is unrealistic.

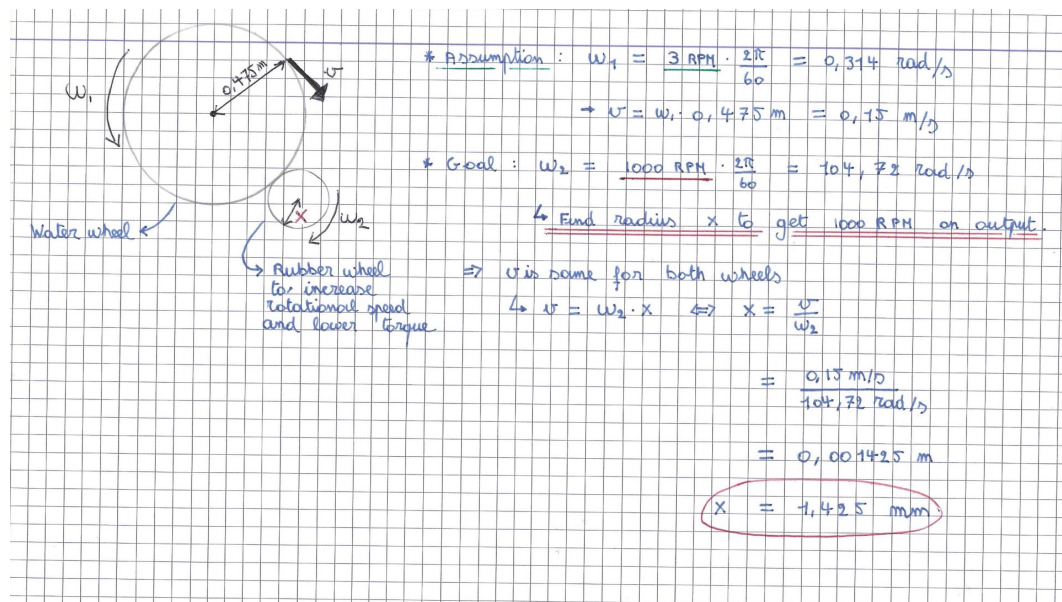


FIGURE D.1: Rubber wheel to increase the rotational speed - calculation

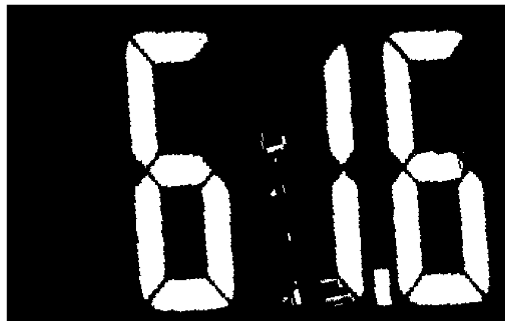
Appendix E

Torque

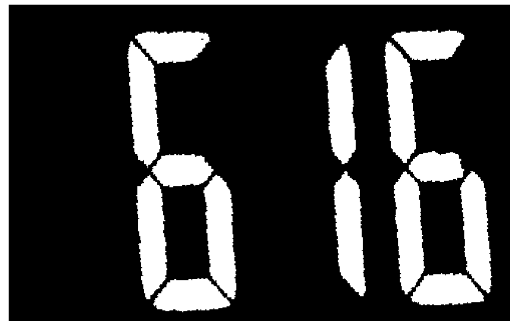
E.1 Seven segment OCR

E.1.1 Preprocessing

Figure E.1 shows the intermediary preprocessing that were omitted from the general discussion as they are considered irrelevant for the understanding of the algorithm.



(A) Crane scale frame - binarised



(B) Crane scale frame - deleted pixels



(C) Crane scale frame - eroded



(D) Crane scale frame - smooth edges

FIGURE E.1: Crane scale frame - intermediate steps

E. TORQUE

E.1.2 Shortcomings

Two shortcomings of the preprocessing are visualised here. Figure E.2 shows the removal of a full digit causing the resulting force value to be one order of magnitude smaller. Figure E.3 shows the removal of half a digit causing the resulting force value to be one order of magnitude larger. Both issues appear when the frame being detected is taken when the screen is in the middle of changing values and are solved in post.

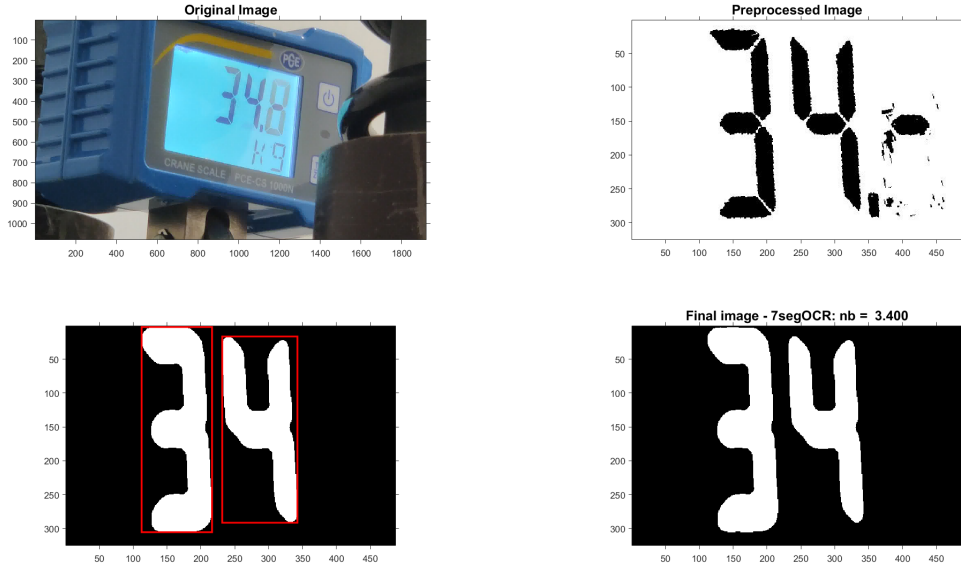


FIGURE E.2: Seven segment OCR - flaw - full digit removed

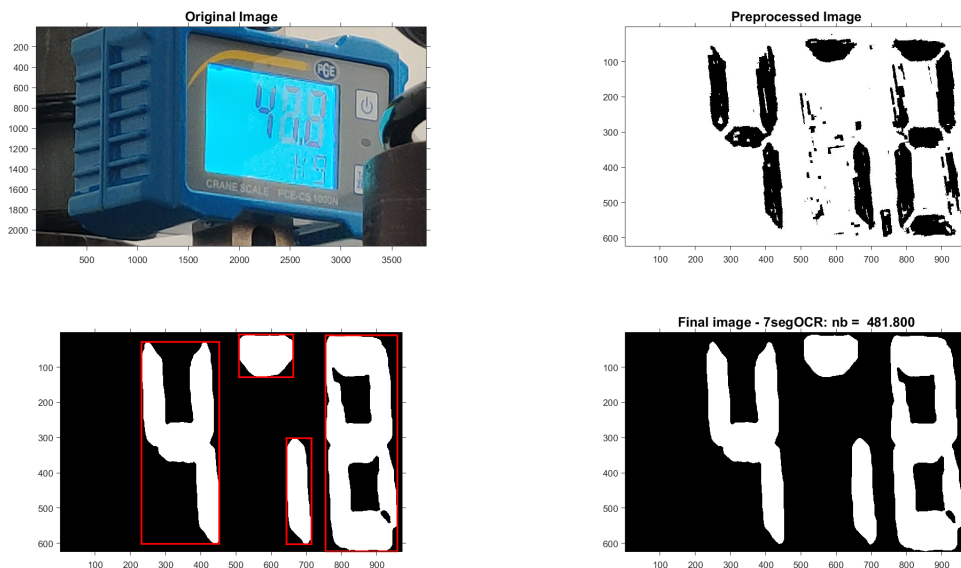


FIGURE E.3: Seven segment OCR - flaw - half of digit removed

E.2 Measurements

Figure E.4 shows the measured torque points without a curve fitted to them. Figure E.5 and E.6 show the residuals of the quadratic fit to them showing no pattern and small values.

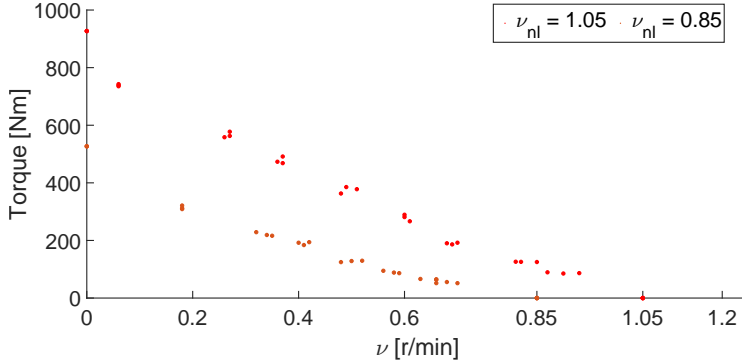


FIGURE E.4: Arenberg water wheel - torque data points

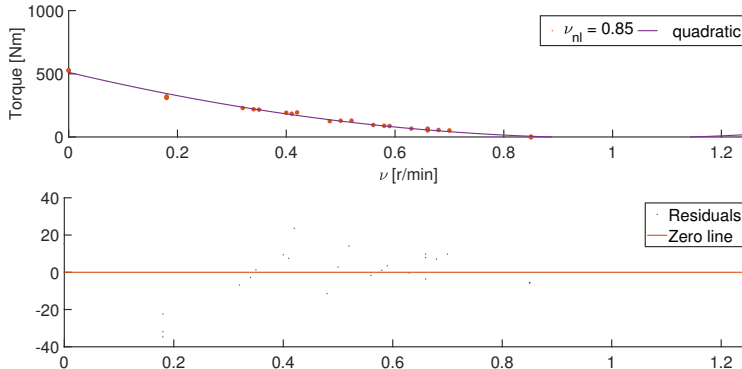


FIGURE E.5: Residuals for quadratic fit for $T_{\nu_{0.85}}$

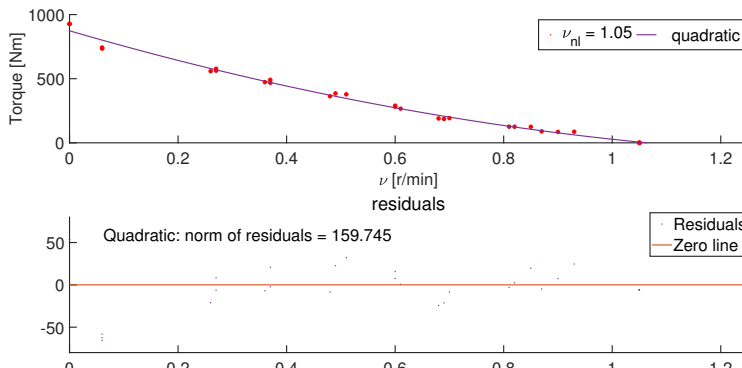


FIGURE E.6: Residuals for quadratic fit for $T_{\nu_{1.05}}$

Appendix F

Website screenshots

Figure F.1 shows the homepage of the Arenberg watermill website and Figure F.2 and F.3 show parts of the real-time page.

The screenshot shows the homepage of the Arenberg Watermill website. At the top, there is a navigation bar with links to Home, Purpose, Real-time data, Measurement module, Water level station, RPM, and Restoration. Below the navigation bar, there is a large image of a watermill. To the right of the image, the word "About" is displayed above a "Hi" greeting with a hand icon. A section titled "Welcome to the official page of the Arenberg Watermill. Look around!" contains text about the restoration project and links to social media and Wikipedia. Below this, there is a map of Europe showing the location of the Arenberg Watermill in Belgium.

Home Purpose Real-time data Measurement module Water level station RPM Restoration

About

Hi

Welcome to the official page of the Arenberg Watermill. Look around!

In September 2020, the historical Arenberg Watermill was restored in its full glory. This website is the result of a thesis investigation performed by engineering student Tibo Geenen, towards the feasibility of green energy generation by the watermill. It shows [real-time data](#) and provides an in-depth look into why it will unfortunately not be able to contribute to the production of renewable electricity.

If you would like to know more about the history of the watermill, there are a few sources provided by the KU Leuven (in Dutch). Firstly an [article](#) before the restauration, then the [campain page](#) to raise funds and lastly an [article](#) after installation of the restored mills (also in [English](#)). Extra footage can be found [here](#) or on the YouTube channel or Wikipedia page.

The mill is located on KU Leuven campus grounds, right next to the stunning Arenberg Castle. The exact location is shown on the map below.

Report a problem | © OpenStreetMap contributors

FIGURE F.1: Arenberg watermill website - homepage

Real-time data

The RPM data shown on this page is real-time and updates every single time a new measurement is detected. It is measured by a custom-made module and includes a local visual representation of the data as well. More information about the module can be found [here](#). If the mill is standing still it will appear as if there are no updates. However, the final [interval block](#) keeps track of the zero values.



Mill 1



FIGURE F.2: Arenberg watermill website - real-time - mill 1

Graph

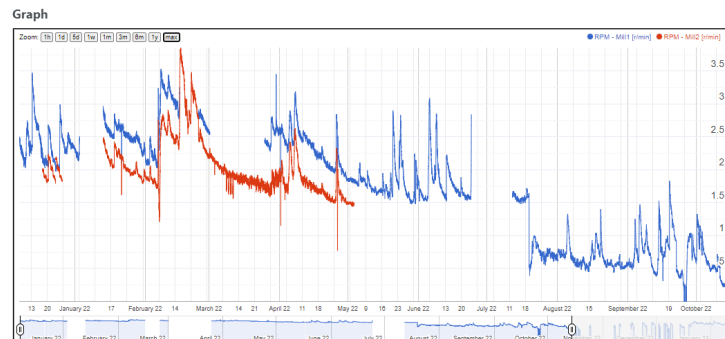


FIGURE F.3: Arenberg watermill website - real-time - graph

Bibliography

- [1] “From where do we import energy?”
<https://ec.europa.eu/eurostat/cache/infographs/energy/bloc-2c.html>, Eurostat.
- [2] “Repowereu: a plan to rapidly reduce dependence on russian fossil fuels and fast forward the green transition,” European Commission, 2022. [Online]. Available: https://ec.europa.eu/commission/presscorner/detail/en/IP_22_3131
- [3] “Fit for 55: how the eu plans to boost renewable energy,”
<https://www.consilium.europa.eu/en/infographics/fit-for-55-how-the-eu-plans-to-boost-renewable-energy/>, European Council.
- [4] “Renewable energy statistics,” Eurostat. [Online]. Available:
https://ec.europa.eu/eurostat/statistics-explained/index.php?title=Renewable_energy_statistics#Wind_and_water_provide_most_renewable_electricity.3B_solar_is_the_fastest-growing_energy_source
- [5] E. Quaranta and R. Revelli, “Gravity water wheels as a micro hydropower energy source: A review based on historic data, design methods, efficiencies and modern optimizations,” *Renewable and Sustainable Energy Reviews*, vol. 97, pp. 414–427, Dec. 2018.
- [6] “Hydropower in europe,” <https://hydropower-europe.eu/about-hydropower-europe/hydropower-energy/>, Hydropower Europe.
- [7] “Renewable energy statistics 2022,” IRENA, Abu Dhabi, 2022.
- [8] O. Paish, “Small hydro power: technology and current status,” *Renewable and Sustainable Energy Reviews*, vol. 6, pp. 537–556, Dec. 2002.
- [9] K. Heider, E. Quaranta, J. M. G. Avilés, J. M. R. Lopez, A. L. Balbo, and J. Scheffran, “Reinventing the wheel – the preservation and potential of traditional water wheels in the terraced irrigated landscapes of the ricote valley, southeast spain,” *Agricultural Water Management*, vol. 259, p. 107240, Jan. 2022.
- [10] “Small and micro hydropower restoration handbook,” European Small Hydropower Association (ESHA), 2014. [Online]. Available: <http://www.restor-hydro.eu/>

- [11] J. Senior, N. Saenger, and G. Müller, “New hydropower converters for very low-head differences,” *JOURNAL OF HYDRAULIC RESEARCH*, vol. 48, no. 6, pp. 703–714, 2010.
- [12] S. C. Simmons and W. D. Lubitz, “Archimedes screw generators for sustainable micro-hydropower production,” *International Journal of Energy Research*, vol. 45, pp. 17 480–17 501, Oct. 2021.
- [13] M. Boura, “Water wheel types,”
<https://commons.wikimedia.org/wiki/Special:Contributions/Malcolm.boura>, Apr. 2017.
- [14] J. A. Senior, “Hydrostatic pressure converters for the exploitation of very low head hydropower potential school of civil engineering and the environment doctor of philosophy hydrostatic pressure converters for the exploitation of very low head hydropower potential,” 2009.
- [15] G. Müller and K. Kauppert, “Performance characteristics of water wheels,” *Journal of Hydraulic Research*, vol. 42, pp. 451–460, 2004.
- [16] M. Denny, “The efficiency of overshot and undershot waterwheels,” *European journal of physics*, vol. 25, no. 2, pp. 193–202, 2004.
- [17] V. Santos, “De geijsterse molen,” 2014.
- [18] “Batheaston old mill,” <http://transitionbath.org/>, Transition Bath, Dec. 2014.
- [19] E. Quaranta and G. Müller, “Sagebien and zuppinger water wheels for very low head hydropower applications,” *Journal of Hydraulic Research*, vol. 56, pp. 526–536, Jul. 2018.
- [20] “Sagebien water wheel quietly generates electricity,”
https://www.gratia-hydro.com/en/32_sagebien_waterwheel.html, Gratia Hydro.
- [21] E. Quaranta and G. Müller, “Optimization of undershot water wheels in very low and variable flow rate applications,” *J. Hydraul. Res.*, vol. 58, no. 5, pp. 845–849, Sep. 2020.
- [22] S. Paudel, M. Weber, D. Geyer, and N. Saenger, “Zuppinger water wheel for very low-head hydropower application,” in *Marine and Hydro Power*. University of Maribor Press, Jul. 2017.
- [23] J. Smeaton, “Xviii. an experimental enquiry concerning the natural powers of water and wind to turn mills, and other machines, depending on a circular motion.” *Philosophical Transactions of the Royal Society of London*, vol. 51, pp. 100–174, Dec. 1759.

BIBLIOGRAPHY

- [24] “Trash racks: Types, installation, and maintenance,” <https://theconstructor.org/water-resources/trash-racks/559412/>, The Constructor.
- [25] “Trash rack cleaner,” <https://www.wild-metal.com/en/trash-rack-cleaner>, Wild Metal.
- [26] T. Saroinsong, R. Soenoko, S. Wahyudi, and M. Sasongko, “Performance of three-bladed archimedes screw turbine,” pp. 9491–9495, Jan. 2016.
- [27] C. D. McNabb, C. R. Liston, and S. M. Borthwick, “Passage of juvenile chinook salmon and other fish species through archimedes lifts and a hidrostal pump at red bluff, california,” *Transactions of the American Fisheries Society*, vol. 132, no. 2, pp. 326–334, 2003. [Online]. Available: [https://doi.org/10.1577/1548-8659\(2003\)132<0326:POJCSA>2.0.CO;2](https://doi.org/10.1577/1548-8659(2003)132<0326:POJCSA>2.0.CO;2)
- [28] Tombek and Holzner, “Untersuchungen zur effektivität alternativer triebwerkstechniken und schutzkonzepte für abwandernde fische beim betrieb von kleinwasserkraftanlagen,” Jan. 2017.
- [29] R. Belmans, G. Deconinck, and J. Driesen, *Elektrische energie*. Acco, 2011.
- [30] J. Meyers, “Lecture slides in renewable energy,” Mar. 2020.
- [31] I. V. Houdenhove, “Toen en nu: Watermolen arenberg,” <https://nieuws.kuleuven.be/nl/2017/toen-nu-watermolen-arenberg>, Nov. 2017.
- [32] “Iconic watermill at the arenberg castle restored,” <https://stories.kuleuven.be/nl/verhalen/watermolen-aan-arenbergkasteel-in-ere-hersteld>, KUL, Sep. 2020.
- [33] “Prospective students,” <https://www.kuleuven.be/english/prospective-students/open-days/online-open-days/faculty-of-engineering-science>, KUL, Dec. 2022.
- [34] R. Stevens, “Watermolen arenberg na restauratie,” 2020.
- [35] E. Awardee, “The sagebien project,” 2001.
- [36] G. Braca, “Stage-discharge relationships in open channels: practices and problems,” Dec. 2022.
- [37] “Station k08_012 data,” https://www.waterinfo.be/station/01K08_012, VMM.
- [38] “Glossary,” https://www.waterinfo.be/?path=NL/Algemene_Info/verklarende_woordenlijst, VMM.
- [39] B. Motten, J. Snaet, and S. Saeys, “De watermolen van het kasteel van arenberg,” Dec. 2014.
- [40] “Zandvang in eghenoven,” https://www.vmm.be/water/beheer-waterlopen/afbeeldingen/zandvang_eghenoven_OK.jpg/view, VMM.

- [41] A. S. Morris and R. Langari, “Rotational motion transducers,” *Measurement and Instrumentation*, pp. 603–636, Jan. 2021.
- [42] N. Matthew and R. Stones, *Beginning Linux Programming*, 4th ed. Wrox Press, Oct. 2007.
- [43] *Extremely Accurate I2C-Integrated RTC*, Maxim Integrated, 2015. [Online]. Available: <https://datasheets.maximintegrated.com/en/ds/DS3231.pdf>
- [44] M. Torfs, “Nooit piekten de dagtemperaturen hoger in België: 2022 op één na warmste jaar,” <https://www.vrt.be/vrtnws/nl/2022/12/20/nooit-piekten-de-temperaturen-hoger-in-belgie-2022-gaat-boeken/>, Dec. 2022.
- [45] “Unbalance: The common cause of vibration,” https://irdproducts.com/unbalance---cause-of-vibration.html#the_importance_of_dynamic_balancing, IRD Balancing, 2021.
- [46] A. Fernandez, “Causes of imbalance,” <https://power-mi.com/content/causes-imbalance>, Power-MI, 2022.
- [47] K. X. Soulis, “Hydrological data sources and analysis for the determination of environmental water requirements in mountainous areas,” *Environmental Water Requirements in Mountainous Areas*, pp. 51–98, Jan. 2021.
- [48] “Coefficient of variation,” <https://datacollection.jrc.ec.europa.eu/wordef/coefficient-of-variation>, European Commission.
- [49] D. M. Stefanescu, *Handbook of force transducers*, 2011th ed. Berlin, Germany: Springer, May 2011.
- [50] T. D. Rybel and G. Deconinck, “Lecture slides in measurement and testing, including high voltages,” Sep. 2020.
- [51] A. S. Morris and R. Langari, “Mass, force, and torque measurement,” *Measurement and Instrumentation*, pp. 547–564, Jan. 2016.
- [52] G. W. Rainer Schiker, *Measuring Torque Correctly*, HBM, 2002.
- [53] D. Fodorean, L. Szabo, and A. Miraoui, “Generator solutions for stand alone pico-electric power plants,” *2009 IEEE International Electric Machines and Drives Conference, IEMDC '09*, pp. 434–438, 2009.
- [54] E. Quaranta, “Investigation and optimization of the performance of gravity water wheels,” 2017.
- [55] G. Müller, H. Williams, K. Atkinson, R. Fleminger, A. Goodwin, and N. A. Harris, “The impulse wheel as hydropower converter for irrigation systems,” *ISH Journal of Hydraulic Engineering*, 2021.

BIBLIOGRAPHY

- [56] Budiarso, Helmizar, Warjito, A. Nuramal, W. Ramadhanu, and D. Adanta, “Performance of breastshot waterwheel in run of river conditions,” *AIP Conference Proceedings*, vol. 2227, May 2020.
- [57] M. Krüger, “Pattern of prony brake,”
<https://commons.wikimedia.org/w/index.php?curid=4494323>, Aug. 2008.
- [58] “China university of mining motor test bench,” <https://made-in-china.com/>, Made in China.
- [59] A. Chaudhuri, K. Mandaviya, P. Badelia, and S. K. Ghosh, *Optical character recognition systems for different languages with soft computing*, 1st ed., ser. Studies in fuzziness and soft computing. Cham, Switzerland: Springer International Publishing, Jan. 2017.
- [60] R. C. Gonzalez and R. E. Woods, *Digital Image Processing*. Prentice Hall, 2022.